Published for SISSA by Springer

Received: *July 8, 2023*
Revised: *October 15, 2023*
Accepted: *November 17, 2023*
Published: *November 27, 2023*

Islands and dynamics at the interface

Mir Afrasiar, Debarshi Basu, Ashish Chandra, Vinayak Raj and Gautam Sengupta

Department of Physics, Indian Institute of Technology, Kanpur 208 016, India

E-mail: afrasiar@iitk.ac.in, debarshi@iitk.ac.in, achandra@iitk.ac.in, vraj@iitk.ac.in, sengupta@iitk.ac.in

Abstract: We investigate a family of models described by two holographic CFT_2s coupled along a shared interface. The bulk dual geometry consists of two AdS_3 spacetimes truncated by a shared Karch-Randall end-of-the-world (EOW) brane. A lower dimensional effective model comprising of JT gravity coupled to two flat CFT_2 baths is subsequently realized by considering small fluctuations on the EOW brane and implementing a partial Randall-Sundrum reduction where the transverse fluctuations of the EOW brane are identified as the dilaton field. We compute the generalized entanglement entropy for bipartite states through the island prescription in the effective lower dimensional picture and obtain precise agreement in the limit of large brane tension with the corresponding doubly holographic computations in the bulk geometry. Furthermore, we obtain the corresponding Page curves for the Hawking radiation in this JT braneworld.

Keywords: AdS-CFT Correspondence, Black Holes, Gauge-Gravity Correspondence

ArXiv ePrint: 2306.12476

https://doi.org/10.1007/JHEP11(2023)192

JHEP11(2023)192

Contents

1 Introduction **1**

2 Review of earlier literature **4**
2.1 JT gravity through dimensional reduction 4
2.2 Interface CFT 6

3 Realising JT gravity at the interface of two spacetimes **7**
3.1 Generalized entropy 12

4 Islands in extremal JT black holes **15**
4.1 Semi-infinite subsystem 16
4.2 Finite subsystem 18
4.2.1 Phase - I 19
4.2.2 Phase - II 20
4.2.3 Phase - III 20
4.2.4 Page curve 24

5 Islands outside eternal JT black holes **24**
5.1 Phase - I 26
5.2 Phase - II 27
5.3 Page curve 28

6 Islands and replica wormholes: gravity coupled with two baths **29**
6.1 Replica wormholes from AdS/ICFT 30
6.2 Replica wormholes with JT gravity coupled to two baths 34

7 Summary and discussion **36**

A Second order fluctuations **37**

JHEP11(2023)192

1 Introduction

In recent years the remarkable progress towards a possible resolution of the black hole information loss paradox in toy models has garnered intense research focus. This development involved a CFT coupled to a theory of gravity where the inclusion of bulk regions termed "*islands*" in the entanglement wedge for subsystems in radiation baths at late times [1–6] ensured that the von Neumann entropy of the Hawking radiation follows the Page curve [7–9]. The crucial ingredient in this island formalism is the incorporation of *replica wormhole*

saddles dominant at late times, in the gravitational path integral for the Rényi entanglement entropy. In [10], based on holographic arguments, a comparison between the island formula in such theories with a CFT coupled to a gravitational theory and the boundary conformal field theory (BCFT) was explored where the authors observed an equivalence between the two. This was dubbed as the *Island-BCFT correspondence*.

A more natural way to understand this island formalism was provided through the *doubly holographic* description [3, 10–20] in which the radiation baths are described by holographic CFTs dual to a bulk geometry. The island formula then emerges from the standard holographic characterization of the entanglement entropy through the (H)RT prescription in the corresponding higher dimensional bulk geometry. This doubly holographic interpretation of the island formula was explored in [21, 22] in the context of an extension of the $AdS_3/BCFT_2$ [11, 12, 23–25] duality through the inclusion of additional *defect* conformal matter on the end-of-the-world (EOW) brane. In this defect $AdS_3/BCFT_2$ framework the equivalence of the quantum corrected RT formula, termed as the defect extremal surface formula, in the $3d$ bulk geometry with the corresponding island formula in the lower dimensional effective $2d$ description could be demonstrated. This doubly holographic description in the $AdS_3/BCFT_2$ framework was further investigated for different mixed state entanglement measures [26–30].

In relation to the above discussion, the Jackiw-Teitelboim (JT) gravity [31, 32] coupled to a radiation bath in two dimensions has proved to be an interesting solvable model to study the application of the island formula [2–5, 33]. Recently in [34], the authors have realised this setup through a dimensional reduction of a defect AdS_3 bulk with small transverse fluctuations on the EOW brane.[1] In particular, they have derived the full JT gravity action through a partial dimensional reduction of the $3d$ bulk wedge sandwiched between a virtual zero tension brane and the finite tension EOW brane, by identifying the transverse fluctuations with the dilaton field in the $2d$ effective description. This has the effect of tweaking the boundary degrees of freedom to obtain the JT gravity in the dual theory. Usual AdS_3/CFT_2 prescription has been utilized in the remaining part of the bulk to obtain the bath CFT_2 on the asymptotic boundary of the AdS_3 geometries. This has provided a $3d$ holographic dual for the JT gravity coupled to a CFT_2 bath.

On a separate note, the doubly holographic description of the island formula has been further investigated in [39] for an interface CFT ($ICFT_2$) [40] where two CFT_2s on half lines with different central charges were considered to be communicating through a common quantum dot. The holographic bulk for such a field theoretic configuration is described by two truncated AdS_3 geometries with different length scales, sewed together along the constant tension EOW brane. In such a configuration, the equivalence between the island formula and the holographic entanglement entropy has been illustrated for certain bipartite states.

In this context, lifting the constraint of the rigidity of the EOW brane in the $ICFT_2$ setup could lead to interesting physics as the gravitational theory on the EOW brane

[1] The authors in [35, 36] had also obtained the JT gravity from Karch-Randall branes in the context of wedge holography, through a similar prescription. Also note that, the authors in [37, 38] had investigated a related prescription to obtain JT black holes through a similar partial dimensional reduction starting from AdS_3 geometries.

JHEP11(2023)192

becomes dynamical and we expect physical quantities e.g. the Page time, to have non-trivial dependence on the gravitational degrees of freedom. However, inspired by the Island/BCFT correspondence, we also expect that the qualitative behaviour of the Page curves will not be affected. Moreover, owing to the restrictions[2] placed on the interface degrees of freedom in the ICFT$_2$ model [39], a naive generalization of the techniques of [34–36] is not obvious and requires careful examination. In the present article this configuration has been investigated where we introduce transverse fluctuations on the EOW brane to obtain the JT gravity through a partial dimensional reduction. In the lower dimensional $2d$ effective perspective, this configuration is described by a JT black hole coupled to two CFT$_2$ baths termed CFT$^{\text{I}}$ and CFT$^{\text{II}}$. In particular, we have two separate CFT$_2$s in the JT background, interacting through the gravity, whereas they remain decoupled on the remaining half lines with fixed geometry. An alternative description of this configuration involves the consideration of the ICFT$_2$ as a holographic dual of the $3d$ bulk where the interface degrees of freedom may now be interpreted as an SYK quantum dot. Naturally the three perspectives described above constitute a double holographic description for this model of JT gravity coupled to two CFT baths.

We investigate the entanglement entropy for various bipartite states for this model described by subsystems in the two CFT baths coupled to JT gravity at zero and finite temperatures. Interestingly for our model we encounter certain novel island configurations absent in the earlier analysis with a single bath [4, 5]. Specifically we demonstrated that there are island contribution from both CFT$^{\text{I}}$ and CFT$^{\text{II}}$ even when the subsystem in question involve only bath degrees of freedom from CFT$^{\text{II}}$ which leads to a modification of the standard island formula involving these *induced islands*. Our results for the entanglement entropy obtained through the above modified island formula in the $2d$ effective picture in the large central charge limit, exactly reproduces the $3d$ bulk computations in the doubly holographic perspective.

As a significant consistency check, we perform a replica wormhole computation for one of the configurations considered above to obtain the position of the conical singularity situated at the boundary of the island region. To this end, we employ the well known conformal welding problem [4, 41, 42] to define a coordinate system consistently spanning the complete hybrid manifold consisting of a gravitational part and two non-gravitating baths. Solving this welding problem reproduces the location of the quantum extremal surface obtained through the extremization of the generalized entropy. It is worth emphasising here that the recovery of the quantum extremal surface from the solution of this welding problem does not assume any holography providing a significant non-trivial consistency check of the island formula for this setup.

The rest of the article is organized as follows. In section 2, we review the basic ingredients of our model, namely, the mechanism of partial dimensional reduction for a defect AdS$_3$ bulk to obtain the JT gravity coupled to a radiation bath, and the salient features of the ICFT$_2$ and its holographic dual. Subsequently, in section 3 we derive the JT gravity

[2]Note that as compared to a BCFT$_2$ [23], the tension of the EOW brane has a smaller range in the ICFT$_2$ setup (cf. eq. (2.14)). This arises from the fact that, unlike a BCFT$_2$, the interface degrees of freedom are constrained by the conformal symmetries of both the CFT$_2$s.

JHEP11(2023)192

coupled to two radiation baths through a partial dimensional reduction of two truncated AdS_3 geometries sewed together along a fluctuating EOW brane. Furthermore, we provide a prescription for the modified island formula in such CFT models. In section 4, we perform the computation for the entanglement entropy for certain configurations in the $2d$ effective description at zero temperature involving extremal JT black holes. Subsequently, in section 5, the computation of the entanglement entropy for subsystems at finite temperature which involve eternal JT black holes is performed. In section 6, we provide the replica wormhole computation for a simple configuration considered earlier and show perfect matching with the island result. Finally in section 7 we summarize our results and present conclusions. Additionally, in appendix A we investigate the second order terms corresponding to the perturbation in the brane tension to obtain the corrections in the bulk on-shell action.

2 Review of earlier literature

2.1 JT gravity through dimensional reduction

In this subsection we review the mechanism to obtain JT gravity through the dimensional reduction of an AdS_3 geometry truncated by a fluctuating EOW brane [34–36]. For this purpose, consider the defect $AdS_3/BCFT_2$ scenario where additional degrees-of-freedom are incorporated at the boundary of the $BCFT_2$ which results in the introduction of defect conformal matter on the EOW brane truncating the AdS_3 spacetime. The gravitational action on the dual bulk manifold $\mathcal{N}$ to such a defect $BCFT_2$ defined on the half line $x \geq 0$ is given by [21, 22, 26–28]

$$I = \frac{1}{16\pi G_N}\int_{\mathcal{N}} \mathrm{d}^3x\sqrt{-g}(R-2\Lambda) + \frac{1}{8\pi G_N}\int_{\mathbb{Q}} \mathrm{d}^2y\sqrt{-h}K + I_{\mathbb{Q}}^{\mathrm{CFT}}\,, \tag{2.1}$$

where h_{ab} is the induced metric and K is the trace of the extrinsic curvature K_{ab} of the EOW brane denoted as $\mathbb{Q}$. The Neumann boundary condition describing the embedding of the EOW brane $\mathbb{Q}$ with the defect conformal matter is given by

$$K_{ab} - h_{ab}K = 8\pi G_N T_{ab}\,, \tag{2.2}$$

where $T_{ab} = -\frac{2}{\sqrt{-h}}\frac{\delta I_{\mathbb{Q}}^{\mathrm{CFT}}}{\delta h^{ab}}$ is the stress energy tensor for the defect CFT_2. The authors in [34] considered the matter action to be of the specific form given by

$$I_{\mathbb{Q}}^{\mathrm{CFT}} = -\frac{1}{8\pi G_N}\int_{\mathbb{Q}} \mathrm{d}^2y\sqrt{-h}T\,, \tag{2.3}$$

where T denotes the brane tension.

A convenient set of coordinates to describe the $3d$ bulk geometry are (t, ρ, y) for which the AdS_3 spacetime is foliated by AdS_2 slices and the metric is given by

$$\mathrm{d}s^2 = \mathrm{d}\rho^2 + L^2\cosh^2\left(\frac{\rho}{L}\right)\frac{-\mathrm{d}t^2+\mathrm{d}y^2}{y^2}\,, \tag{2.4}$$

JHEP11(2023)192

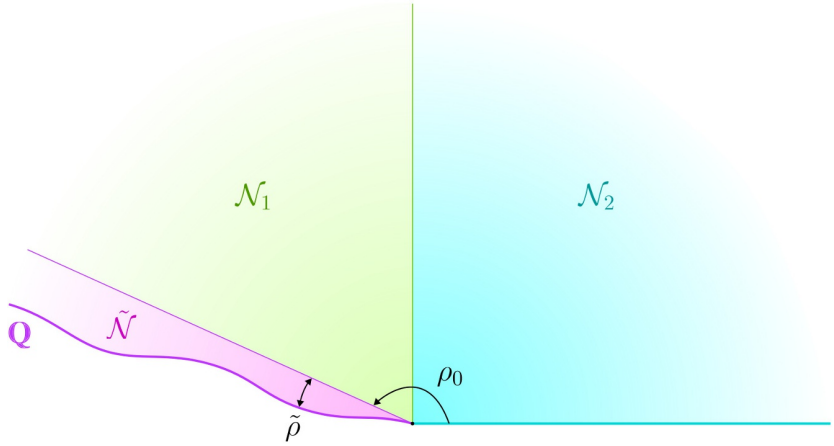

Figure 1. Schematics of the partial dimensional reduction of the AdS/BCFT setup with a fluctuating EOW brane $\mathbb{Q}$. Figure modified from [34].

where L is the AdS_3 radius. The constant tension T of the brane in these coordinates may then be obtained to be

$$T = \frac{\tanh \frac{\rho_0}{L}}{L} \tag{2.5}$$

where ρ_0 is the location of the brane $\mathbb{Q}$.

The EOW brane $\mathbb{Q}$ is now made dynamical by introducing a coordinate dependent perturbation of the form [34, 35]

$$\rho = \rho_0 + \tilde{\rho}\,, \tag{2.6}$$

where $\tilde{\rho}$ is a small fluctuation such that $\frac{\tilde{\rho}}{\rho_0} \ll 1$. For the specific form of the metric in eq. (2.4), it is possible to integrate out the ρ direction in the bulk for the wedge region $\mathcal{N}_1 + \tilde{\mathcal{N}}$ as shown in figure 1. Dimensional reduction for the region $\mathcal{N}_2$ in the ρ direction will give the original CFT_2 on the asymptotic boundary of the AdS_3 bulk through the usual AdS/CFT correspondence.

Now performing this partial dimensional reduction for the bulk gravitational action given in eq. (2.1) for the wedge region $\mathcal{N}_1 + \tilde{\mathcal{N}}$, one may obtain the action for the $2d$ effective theory as follows [34]

$$I_{2d} = \frac{\rho_0}{16\pi G_N}\int_{\mathbb{Q}} \mathrm{d}^2y\sqrt{-g^{(2)}}R^{(2)} + \frac{\rho_0}{16\pi G_N}\int_{\mathbb{Q}} \mathrm{d}^2y\sqrt{-g^{(2)}}\frac{\tilde{\rho}}{\rho_0}\left(R^{(2)} + \frac{2}{L^2\cosh^2\left(\frac{\rho_0}{L}\right)}\right) + \dots\,, \tag{2.7}$$

where $g^{(2)}_{ab}$ describes the AdS_2 metric with the length scale $L\cosh\left(\frac{\rho_0}{L}\right)$, $R^{(2)}$ is the scalar curvature corresponding to $g^{(2)}_{ab}$ and ellipsis denote $\mathcal{O}\left(\tilde{\rho}^2/\rho_0^2\right)$ terms in the perturbative expansion. The $3d$ Newton's constant G_N is related to that in the $2d$ effective theory $G^{(2)}_N$ as follows [10, 21]

$$\frac{1}{G^{(2)}_N} = \frac{\rho_0}{G_N}\,. \tag{2.8}$$

It should be noted here that in eq. (2.7), the tension of the EOW brane is considered to be the same as in eq. (2.5) as the fluctuation (2.6) only changes the tension up to $\mathcal{O}(\frac{\tilde{\rho}^3}{\rho_0^3})$.

JHEP11(2023)192

Remarkably, eq. (2.7) describes the JT gravity action modulo certain boundary terms[3] on identification of $\frac{\tilde{\rho}}{\rho_0}$ with the dilaton field. This provides us with a mechanism for obtaining JT gravity as a $2d$ effective theory through the partial dimensional reduction of an AdS_3 geometry with a fluctuating EOW brane.

2.2 Interface CFT

In this subsection, we review a class of interface CFT_2s ($ICFT_2$s) first discussed in [40]. It was recently studied by the authors in [39] which involves two CFT_2s defined on half lines coupled through a quantum dot. The bulk dual for such a theory is described by two locally AdS_3 geometries separated by a permeable EOW brane. The two CFT_2s located at the asymptotic boundary of the AdS_3 geometries are labelled as CFT^{I} and CFT^{II} with central charges c_{I} and c_{II} respectively, and the corresponding dual bulk locally AdS_3 geometries are labelled as AdS^{I} and AdS^{II} with length scales L_{I} and L_{II} respectively. In the semi-classical approximation, there is also an intermediate $2d$ effective perspective to describe this configuration, which may be obtained by integrating out bulk degrees of freedom. This results in the brane being characterized by a weakly gravitating system coupled to the original $CFT^{I,II}$s. This $2d$ effective perspective will be discussed in detail in section 3 in the context of the JT gravity on the EOW brane.

The action for the dual bulk geometry describing the above configuration is given by [39]

$$\begin{aligned} I = &\frac{1}{16\pi G_N}\left[\int_{\mathcal{B}_{I}} \mathrm{d}^3x\sqrt{-g_{I}}\left(R_{I}+\frac{2}{L_{I}^2}\right)+\int_{\mathcal{B}_{II}} \mathrm{d}^3x\sqrt{-g_{II}}\left(R_{II}+\frac{2}{L_{II}^2}\right)\right] \\ &+\frac{1}{8\pi G_N}\left[\int_{\Sigma}\mathrm{d}^2y\sqrt{-h}(K_{I}-K_{II})-T\int_{\Sigma}\mathrm{d}^2y\sqrt{-h}\right], \end{aligned} \tag{2.9}$$

where h_{ab} is the induced metric and T is the tension of the EOW brane Σ. The relative minus sign between the two extrinsic curvatures $K_{I,II}$ is due to the fact that the outward normal is always taken to be pointing from the AdS^{I} to the AdS^{II} geometry. The properties of the EOW brane is fixed by requiring it to satisfy certain junction conditions. The first of these demands that the induced metric h_{ab} on the brane be the same as viewed from either of the two $AdS_3^{I,II}$ geometries. The second is the Israel junction condition for the brane with the two $AdS_3^{I,II}$ geometries on either side which may be expressed as [39]

$$(K_{I,ab}-K_{II,ab})-h_{ab}(K_{I}-K_{II})=-T\,h_{ab}\,. \tag{2.10}$$

Solving these junction conditions will require us to specify the coordinate system describing the $3d$ geometry. To this end, the AdS_2 foliation of the AdS_3 geometry is chosen

[3]For the recovery of the complete JT action (including the boundary term), see [34].

JHEP11(2023)192

again on each patch of the spacetime $\mathcal{B}_{\rm I,II}$ as follows[4]

$$\begin{aligned} \mathrm{d}s^2_{\mathcal{B}_k} &= \mathrm{d}\rho_k^2 + L_k^2 \cosh^2\left(\frac{\rho_k}{L_k}\right) \tilde{h}_{ab}\, \mathrm{d}y^a \mathrm{d}y^b \\ &\equiv \mathrm{d}\rho_k^2 + L_k^2 \cosh^2\left(\frac{\rho_k}{L_k}\right) \frac{-\mathrm{d}t_k^2 + \mathrm{d}y_k^2}{y_k^2}\,, \qquad k = \mathrm{I,II}\,. \end{aligned} \tag{2.12}$$

Here $\tilde{h}_{ab}$ describes the usual Poincaré AdS_2 metric with unit radius. In these coordinates, the EOW brane is considered to be located at $\rho_k = \rho_k^0$ for $k = \mathrm{I,II}$. The first junction condition thus implies the identification of y_k and t_k for both the coordinate patches. Additionally it also enforces the two AdS_2 radii to be the same i.e.,

$$L_{\rm I}^2 \cosh^2\left(\frac{\rho_{\rm I}^0}{L_{\rm I}}\right) = L_{\rm II}^2 \cosh^2\left(\frac{\rho_{\rm II}^0}{L_{\rm II}}\right)\,. \tag{2.13}$$

The solution to the second junction condition (2.10) fixes the position of the EOW brane as follows [39]

$$\tanh\left(\frac{\rho_{\rm I}^0}{L_{\rm I}}\right) = \frac{L_{\rm I}}{2T}\left(T^2 + \frac{1}{L_{\rm I}^2} - \frac{1}{L_{\rm II}^2}\right)\,, \qquad \tanh\left(\frac{\rho_{\rm II}^0}{L_{\rm II}}\right) = \frac{L_{\rm II}}{2T}\left(T^2 - \frac{1}{L_{\rm I}^2} + \frac{1}{L_{\rm II}^2}\right)\,. \tag{2.14}$$

Notice from the above that the tension T of the brane has an upper as well as a lower bound. In the large tension limit described by

$$T \to T_{\rm max} = \frac{1}{L_{\rm I}} + \frac{1}{L_{\rm II}}\,, \tag{2.15}$$

the EOW brane approaches the extended asymptotic boundary of both the AdS_k patches. In this limit, integrating out the bulk degrees of freedom on either side results in the two CFT_2s interacting through the weakly gravitating brane. This is the intermediate $2d$ effective scenario mentioned earlier which will be discussed in detail in the following section in the context of the JT gravity on the EOW brane.

3 Realising JT gravity at the interface of two spacetimes

In this section, we employ a combination of a partial Randall-Sundrum reduction and the usual AdS/CFT correspondence [21, 22, 26–28, 34] to the AdS/ICFT setup described in the preceding subsection, while allowing for small transverse fluctuations of the EOW brane Σ. This procedure results in a two dimensional effective theory comprising of the JT gravity on the EOW brane Σ coupled to two non-gravitating bath CFT_2s. The gravity theory on the brane is obtained by integrating out the bulk AdS_3 geometry near the brane and may

[4] Here ρ is a hyperbolic angular coordinate which can be related to the usual angle χ as follows

$$\tanh\left(\frac{\rho_k}{L_k}\right) \equiv \sin\chi_k. \tag{2.11}$$

In the rest of the article, the location of the brane at ρ_k^0 in this coordinate is represented by $\chi_k = \psi_k$.

JHEP11(2023)192

be thought of as the "bulk dual" of the interface degrees of freedom. On introducing the transverse fluctuations the locations of the EOW brane is described as follows[5]

$$\begin{aligned}\Sigma \ : \ \rho_{\rm I} &= \rho_{\rm I}^0 - \tilde{\rho}_{\rm I}(y) \\ \rho_{\rm II} &= \rho_{\rm II}^0 + \tilde{\rho}_{\rm II}(y)\,.\end{aligned} \tag{3.1}$$

The schematics of the setup is depicted in figure 2. In the above equation, $\tilde{\rho}_k(y) \ll \rho_k^0$ are the small transverse fluctuations away from the brane angle ρ_k^0. Note that the fluctuation modes are functions of the braneworld coordinates y and are treated as fields on the braneworld, as described in [34, 36]. As depicted in figure 2, we may divide the two AdS_3 geometries on either side of the EOW brane, into the wedges $W_k^{(1)}$ and $W_k^{(2)}$. With the fluctuations of the brane turned on, the wedge $W_{\rm II}^{(1)}$ is extended further to include the small wedge region[6] $\tilde{W}$ which is excised out of the wedge region $W_{\rm I}^{(1)}$. Note that, in this setup the AdS_3 spacetimes on either sides of the brane are composed of several wedges as follows

$$\begin{aligned}\mathcal{B}_{\rm I} &= W_{\rm I}^{(1)} \cup W_{\rm I}^{(2)} \setminus \tilde{W}\,, \\ \mathcal{B}_{\rm II} &= W_{\rm II}^{(1)} \cup W_{\rm II}^{(2)} \cup \tilde{W}\,.\end{aligned}$$

We now employ the partial dimensional reduction in the wedge regions $W_{\rm I}^{(1)} \setminus \tilde{W}$ in the $AdS_3^{\rm I}$ and $W_{\rm II}^{(1)} \cup \tilde{W}$ in the $AdS_3^{\rm II}$ geometries by integrate out the bulk AdS_3 degrees of freedom in the $\rho_{\rm I,II}$ direction(s). On the other hand, in the wedges $W_k^{(2)}$, we utilize the standard AdS_3/CFT_2 correspondence which leads to flat non-gravitating CFT_2s on the half lines stretching out from the interface. Note that in the following analysis we consider large ρ_k^0 which restricts us in the large tension regime $T \to T_{\rm max}$ of the AdS/ICFT setup as advocated in [39]. In this limit, the EOW brane Σ is pushed towards the asymptotic boundaries of each AdS_3 geometry and hence the AdS_3 isometries are reminiscent of the conformal transformations on the brane. Therefore, it is natural to expect a gravitational theory coupled to the two bath CFT_2s to emerge in the lower dimensional effective description obtained from the partial dimensional reduction. In the following, we investigate the nature of this gravitational theory by explicitly integrating out the bulk AdS_3 geometries.

The three-dimensional bulk Ricci scalars are related to the $2d$ Ricci scalar $R^{(2)}$ on the brane Σ as follows

$$\sqrt{-g_k}R_k = \sqrt{-g^{(2)}}\left[R^{(2)} - \frac{2\left(3\cosh^2\left(\frac{\rho_k}{L_k}\right)-1\right)}{L_k^2\cosh^2\left(\frac{\rho_k^0}{L_k}\right)}\right]\,, \tag{3.2}$$

[5]Note that the fluctuations of the brane angles $\tilde{\rho}_{\rm I}(y)$ and $\tilde{\rho}_{\rm II}(y)$ are not independent degrees of freedom as they describe the same fluctuations as seen from either side of the brane. The explicit relation between $\tilde{\rho}_{\rm I}$ and $\tilde{\rho}_{\rm II}$ may be obtained by identifying the metric on the brane induced from each AdS_3 spacetime (cf. appendix A).

[6]Note that the fluctuations of the EOW brane are completely arbitrary in this setting and may as well excise a portion of the wedge $W_{\rm II}^{(1)}$ from the $AdS_3^{\rm II}$ instead.

JHEP11(2023)192

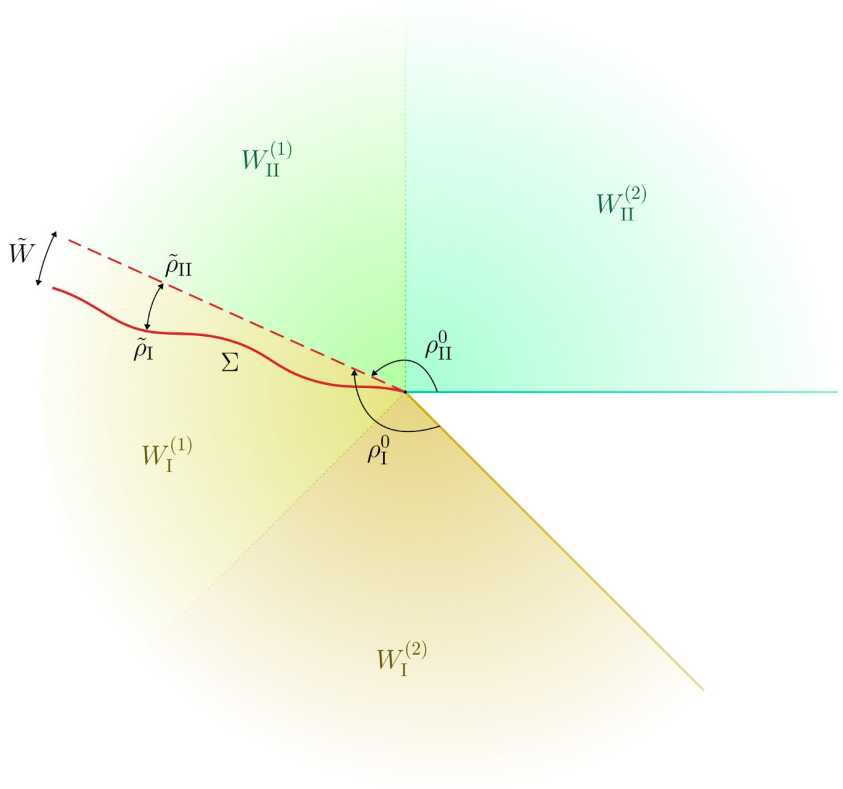

Figure 2. Schematics of the partial dimensional reduction of the AdS/ICFT setup with a fluctuating EOW brane Σ.

where we have utilized the metric in eq. (2.12) upto leading order with

$$g_{ab}^{(2)} = L_k^2 \cosh^2\left(\frac{\rho_k^0}{L_k}\right) \tilde{h}_{ab}\,. \tag{3.3}$$

Integrating the $3d$ bulk Einstein-Hilbert actions (cf. eq. (2.9)) of the $\mathrm{AdS}_3^{\mathrm{I,II}}$ regions inside the wedges $W_{\rm I}^{(1)} \setminus \tilde{W}$ and $W_{\rm II}^{(1)} \cup \tilde{W}$ leads to

$$\begin{aligned}
&\frac{1}{16\pi G_N}\int_{W_{\rm I}^{(1)}\setminus\tilde{W}} \mathrm{d}^3x\sqrt{-g_{\rm I}}\left(R_{\rm I}+\frac{2}{L_{\rm I}^2}\right) + \frac{1}{16\pi G_N}\int_{W_{\rm II}^{(1)}\cup\tilde{W}} \mathrm{d}^3x\sqrt{-g_{\rm II}}\left(R_{\rm II}+\frac{2}{L_{\rm II}^2}\right)\\
&= \frac{1}{16\pi G_N}\int_\Sigma \mathrm{d}^2y\sqrt{-g^{(2)}}\left[\left(\rho_{\rm I}^0-\tilde{\rho}_{\rm I}(y)\right)R^{(2)} - \frac{\sinh\left(\frac{2\rho_{\rm I}^0-2\tilde{\rho}_{\rm I}(y)}{L_{\rm I}}\right)}{L_{\rm I}\cosh^2\left(\frac{\rho_{\rm I}^0}{L_{\rm I}}\right)}\right]\\
&\quad + \frac{1}{16\pi G_N}\int_\Sigma \mathrm{d}^2y\sqrt{-g^{(2)}}\left[\left(\rho_{\rm II}^0+\tilde{\rho}_{\rm II}(y)\right)R^{(2)} - \frac{\sinh\left(\frac{2\rho_{\rm II}^0+2\tilde{\rho}_{\rm II}(y)}{L_{\rm II}}\right)}{L_{\rm II}\cosh^2\left(\frac{\rho_{\rm II}^0}{L_{\rm II}}\right)}\right]\,.
\end{aligned} \tag{3.4}$$

Next, we focus on the Gibbons-Hawking boundary terms and the tension term in eq. (2.9). The extrinsic curvatures $K_{\rm I,II}$ may be computed using the outward normal vector pointing

JHEP11(2023)192

to I $\to$ II as follows

$$K_{\mathrm{I},ab} = \frac{1}{L_{\mathrm{I}}}\tanh\left[\frac{\rho^0_{\mathrm{I}} - \tilde{\rho}_{\mathrm{I}}(y)}{L_{\mathrm{I}}}\right] h_{ab}, \quad K_{\mathrm{II},ab} = -\frac{1}{L_{\mathrm{II}}}\tanh\left[\frac{\rho^0_{\mathrm{II}} + \tilde{\rho}_{\mathrm{II}}(y)}{L_{\mathrm{II}}}\right] h_{ab}\,, \tag{3.5}$$

where h_{ab} is the induced metric on the brane

$$h_{ab} = L_k^2\cosh^2\left(\frac{\rho_k}{L_k}\right)\tilde{h}_{ab}\,, \tag{3.6}$$

and $\tilde{h}_{ab}$ is as defined in eq. (2.12). We keep the tension of the fluctuating brane constant as given in eq. (2.14), perturbatively in $\tilde{\rho}_k$. This may be interpreted as the tension of the brane remaining intact under small transverse fluctuations. Hence, the Gibbons-Hawking boundary term together with the brane tension term leads to

$$\begin{aligned}
&\frac{1}{8\pi G_N}\left[\int_\Sigma \mathrm{d}^2y\sqrt{-h}(K_{\mathrm{I}} - K_{\mathrm{II}}) - T\int_\Sigma \mathrm{d}^2y\sqrt{-h}\right] \\
&= \frac{1}{8\pi G_N}\int_\Sigma \mathrm{d}^2y\sqrt{-g^{(2)}}\left[\frac{\sinh\left(\frac{2\rho^0_{\mathrm{I}} - 2\tilde{\rho}_{\mathrm{I}}(y)}{L_{\mathrm{II}}}\right)}{L_{\mathrm{I}}\cosh^2\left(\frac{\rho^0_{\mathrm{I}}}{L_{\mathrm{I}}}\right)} - \frac{\tanh\left(\frac{\rho^0_{\mathrm{I}}}{L_{\mathrm{I}}}\right)\cosh^2\left(\frac{\rho^0_{\mathrm{I}} - \tilde{\rho}_{\mathrm{I}}(y)}{L_{\mathrm{II}}}\right)}{L_{\mathrm{I}}\cosh^2\left(\frac{\rho^0_{\mathrm{I}}}{L_{\mathrm{I}}}\right)}\right] \\
&\quad + \frac{1}{8\pi G_N}\int_\Sigma \mathrm{d}^2y\sqrt{-g^{(2)}}\left[\frac{\sinh\left(\frac{2\rho^0_{\mathrm{II}} + 2\tilde{\rho}_{\mathrm{II}}(y)}{L_{\mathrm{II}}}\right)}{L_{\mathrm{II}}\cosh^2\left(\frac{\rho^0_{\mathrm{II}}}{L_{\mathrm{II}}}\right)} - \frac{\tanh\left(\frac{\rho^0_{\mathrm{II}}}{L_{\mathrm{II}}}\right)\cosh^2\left(\frac{\rho^0_{\mathrm{II}} + \tilde{\rho}_{\mathrm{II}}(y)}{L_{\mathrm{II}}}\right)}{L_{\mathrm{II}}\cosh^2\left(\frac{\rho^0_{\mathrm{II}}}{L_{\mathrm{II}}}\right)}\right].
\end{aligned} \tag{3.7}$$

Adding the contributions from eqs. (3.4) and (3.7) and expanding perturbatively in small $(\tilde{\rho}_k/\rho^0_k)$ the total bulk action for the lower dimensional effective gravitational theory on the brane Σ, upon partial dimensional reduction on the wedges $W^{(1)}_{\mathrm{I}} \setminus \tilde{W}$ and $W^{(1)}_{\mathrm{II}} \cup \tilde{W}$, becomes

$$\begin{aligned}
I_{\text{total}} = {}& \frac{\rho^0_{\mathrm{I}} + \rho^0_{\mathrm{II}}}{16\pi G_N}\int_\Sigma \mathrm{d}^2y\sqrt{-g^{(2)}}R^{(2)} - \frac{1}{16\pi G_N}\int_\Sigma \mathrm{d}^2y\sqrt{-g^{(2)}}\,\tilde{\rho}_{\mathrm{I}}(y)\left[R^{(2)} + \frac{2}{L_{\mathrm{I}}^2\cosh^2\left(\frac{\rho^0_{\mathrm{I}}}{L_{\mathrm{I}}}\right)}\right] \\
&+ \frac{1}{16\pi G_N}\int_\Sigma \mathrm{d}^2y\sqrt{-g^{(2)}}\,\tilde{\rho}_{\mathrm{II}}(y)\left[R^{(2)} + \frac{2}{L_{\mathrm{II}}^2\cosh^2\left(\frac{\rho^0_{\mathrm{II}}}{L_{\mathrm{II}}}\right)}\right],
\end{aligned} \tag{3.8}$$

where we have neglected terms of order $(\tilde{\rho}_k/\rho^0_k)^2$. See appendix A, for a discussion on the higher order corrections. Utilizing eq. (2.13), the above action may be rewritten in the instructive form

$$I_{\text{total}} = \frac{1}{16\pi G_N^{(2)}}\left[\int_\Sigma \mathrm{d}^2y\sqrt{-g^{(2)}}\,R^{(2)} + \int_\Sigma \mathrm{d}^2y\sqrt{-g^{(2)}}\,\Phi(y)\left(R^{(2)} + \frac{2}{\ell^2_{\text{eff}}}\right)\right], \tag{3.9}$$

where we have defined the two dimensional Newton's constant $G_N^{(2)}$ and the curvature scale ℓ_{eff} on the brane Σ as follows

$$\frac{1}{G_N^{(2)}} = \frac{\rho^0_{\mathrm{I}} + \rho^0_{\mathrm{II}}}{G_N}, \quad \ell_{\text{eff}} = L_{\mathrm{I}}\cosh\left(\frac{\rho^0_{\mathrm{I}}}{L_{\mathrm{I}}}\right) = L_{\mathrm{II}}\cosh\left(\frac{\rho^0_{\mathrm{II}}}{L_{\mathrm{II}}}\right). \tag{3.10}$$

JHEP11(2023)192

Furthermore, in eq. (3.9), we have identified the dilaton field $\Phi(y)$ on the brane with the fluctuations of the brane angles $\tilde{\rho}_k(y)$ as follows[7]

$$\Phi(y) = \frac{\tilde{\rho}_{\rm II}(y) - \tilde{\rho}_{\rm I}(y)}{\rho^0_{\rm I} + \rho^0_{\rm II}} \,. \tag{3.12}$$

With these identifications, the $2d$ bulk action in eq. (3.9) precisely takes the form of the action for JT gravity modulo certain boundary terms, with the topological part of the dilaton field Φ_0 set equal to unity. Furthermore, variation of the action with respect to the dilaton field $\Phi(y)$ leads to the Ricci scalar as

$$R^{(2)} = -\frac{2}{\ell^2_{\rm eff}} = -\frac{2}{L_k^2 \cosh^2\left(\frac{\rho^0_k}{L_k}\right)}, \quad k = \text{I,II} \tag{3.13}$$

which correctly conforms to the fact that the brane is situated at a particular AdS_2 slice as seen from either of the bulk AdS_3 spacetimes.

At this point we recall that, in the limit of large ρ^0_k the EOW brane Σ is pushed towards the asymptotic boundary of each AdS_3 spacetime. In this limit the tension of the brane is also large, $T \to T_{\rm max}$ [39]. As described in [13, 44], in this limit one obtains a non-local action [45] instead of the first term in eq. (3.9) as follows

$$I_{\text{non-local}} = \sum_{k=\text{I,II}} \frac{L_k}{32\pi G_N} \int_\Sigma \mathrm{d}^2 y \sqrt{-\tilde{h}} \left[R^{(2)} - R^{(2)} \log\left(-\frac{L_k^2}{2} R^{(2)} \right) \right] . \tag{3.14}$$

By introducing two auxiliary scalar fields φ_k $(k = \text{I}\,, \text{II})$, the above mentioned non-local action may be rewritten in a local form in terms of the usual Polyakov action[8] as discussed in [39]

$$I_{\rm Poly} = \sum_{k=\text{I,II}} \frac{L_k}{32\pi G_N} \int_\Sigma \mathrm{d}^2 y \sqrt{-\tilde{h}} \left[-\frac{1}{2} \tilde{h}^{ab} \nabla_a \varphi_k \nabla_b \varphi_k + \varphi_k R^{(2)} - \frac{2}{L_k^2}\, e^{-\varphi_k} \right] . \tag{3.15}$$

We may interpret the above Polyakov action as two CFT_2s[9] with central charges $c_{\rm I}$ and $c_{\rm II}$ located on the AdS_2 brane [39]. The JT gravity on the brane is coupled to these CFT_2s which are also identical to the two bath CFT_2s on the two half lines obtained via the standard $\text{AdS}_3/\text{CFT}_2$ dictionary on the bulk wedges $W_k^{(2)}$. In other words, we have two

[7] Note that, in order to break the asymptotic conformal symmetry, we need to introduce a cutoff scale $\epsilon \ll 1$ such that the boundary value of the dilaton reads [43],

$$\Phi(y)\big|_{\rm bdy} = \frac{\Phi_r}{\epsilon} \tag{3.11}$$

where Φ_r is the renormalized coupling. Since we require the brane fluctuations $\tilde{\rho}_k(y)$ to be small when we approach the asymptotic boundary, we have to set $\Phi_r \sim \epsilon^2$ as seen from eq. (3.12). We thank the anonymous reviewer for suggesting this clarification, along the lines of [35, 36].

[8] Note that a similar Polyakov action was obtained via covariantization of the induced Liouville action for the gravity theory in the Island/BCFT correspondence described in [10].

[9] As explained in [39], the nature of the bulk quantum matter on the brane becomes conformal in the large ρ^0_k limit.

JHEP11(2023)192

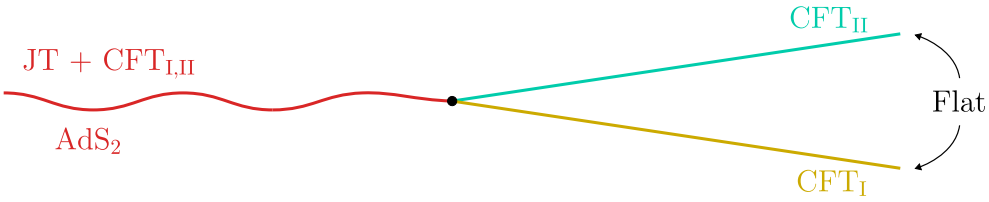

Figure 3. Schematics of the $2d$ effective theory comprised of JT gravity coupled to two flat CFT$_2$ baths.

CFT$_2$s defined on the whole real line. In half of the lines the CFT$_2$s live on a curved AdS$_2$ manifold that is the brane, and are coupled to each other via the JT gravity on this curved manifold. In the other half, the CFT$_2$s live on two flat non-gravitating manifolds and hence are decoupled. The schematics of this $2d$ effective scenario is sketched in figure 3.

To illustrate the emergence of the two CFT$_2$s on the brane via the Polyakov action in eq. (3.15), we note that the zero-dimensional analogue of the transverse area of a codimension two surface $\mathcal{X}$ on the brane is given, for the action eq. (3.15), by [44]

$$\mathcal{A}(\mathcal{X}) = \frac{\Phi(\mathcal{X})}{4G_N^{(2)}} + \frac{1}{8G_N}\sum_{k=\rm I,II} L_k\,\varphi_k(\mathcal{X})\,. \tag{3.16}$$

For the brane Σ situated at the AdS$_2$ slice described by eq. (3.13), the auxiliary scalar fields φ_k may be obtained as [13]

$$\varphi_k = \log\left[-\frac{2}{L_k^2 R^{(2)}}\right] = 2\,\log\left[\cosh\left(\frac{\rho_k^0}{L_k}\right)\right]\,, \tag{3.17}$$

and hence the area term in eq. (3.16) is given by

$$\mathcal{A}(\mathcal{X}) = \frac{\Phi(\mathcal{X})}{4G_N^{(2)}} + \frac{c_{\rm I}}{6}\log\left(\frac{1}{\cos\psi_{\rm I}}\right) + \frac{c_{\rm II}}{6}\log\left(\frac{1}{\cos\psi_{\rm II}}\right)\,, \tag{3.18}$$

where we have utilized eq. (2.11).

To conclude we have obtained an effective intermediate braneworld description involving the JT gravity on a dynamical manifold coupled with two bath CFT$_2$s through a dimensional reduction of a $3d$ bulk which could be understood as a doubly holographic description for the effective $2d$ theory. Recall that this $3d$ bulk has a holographic dual described by an interface CFT where the interface degrees of freedom may be interpreted as an SYK quantum dot.

3.1 Generalized entropy

Consider a QFT coupled to a gravitational theory on an hybrid manifold $\mathcal{M} = \Sigma \cup \mathcal{M}^{\rm I} \cup \mathcal{M}^{\rm II}$, where Σ corresponds to the dynamical EOW brane in the doubly holographic $3d$ description which smoothly joins with the two non-gravitating flat baths[10] $\mathcal{M}^{\rm I,II}$. Transparent boundary conditions are imposed at the common boundary of Σ and $\mathcal{M}^{\rm I,II}$ such

[10]Note that $\mathcal{M}^{\rm I,II}$ forms part of the asymptotic boundary of the $3d$ bulk spacetime, $\partial\mathcal{B}^{\rm I,II} \equiv \Sigma \cup \mathcal{M}^{\rm I,II}$.

JHEP11(2023)192

that the quantum matter fields freely propagate across this boundary. The generalized Rényi entropy for a subsystem A on this hybrid manifold could be obtained through a path integral on the replicated geometry $\mathcal{M}_n = \Sigma_n \cup \mathcal{M}_n^{\rm I} \cup \mathcal{M}_n^{\rm II}$ with branch cuts at the endpoints of A as follows

$$(1-n)S_{\rm gen}^{(n)}(A) = \log {\rm Tr}\boldsymbol{\rho}_A^n = \log \frac{\mathbf{Z}\left[\mathcal{M}_n\right]}{\left(\mathbf{Z}\left[\mathcal{M}_1\right]\right)^n}\,, \tag{3.19}$$

where $\boldsymbol{\rho}_A$ is the reduced density matrix for A in the full quantum theory and $\mathbf{Z}[\mathcal{M}_n]$ corresponds to the partition function of the manifold $\mathcal{M}_n$. Under the semiclassical approximation, the gravitational path integral could be approximated near its saddle point to obtain the partition function on the replicated manifold $\mathcal{M}_n$ as follows

$$\mathbf{Z}\left[\mathcal{M}_n\right] \approx e^{-{\rm I}_{\rm grav}[\Sigma_n]}\,\mathbf{Z}_{\rm mat}\left[\mathcal{M}_n\right]\,, \tag{3.20}$$

where $\mathbf{Z}_{\rm mat}\left[\mathcal{M}_n\right]$ in the matter partition function on the entire replicated hybrid manifold $\mathcal{M}_n$ while ${\rm I}_{\rm grav}\left[\Sigma_n\right]$ is the classical gravitational action on the dynamical manifold Σ_n.

If the replica symmetry for the bulk saddle point configuration in the semiclassical approximation remains intact, the orbifold $\tilde{\mathcal{M}}_n \equiv \mathcal{M}_n/\mathbb{Z}_n$ obtained by quotienting via the replica symmetry $\mathbb{Z}_n$ contains conical defects with deficit angle $\Delta\phi_n = 2\pi(1-1/n)$ along the replica fixed points in the bulk geometry. This is the so-called *replica wormhole* saddle discussed in the literature [2–5]. The region enclosed between these conical singularities in the bulk constitute the island ${\rm Is}(A)$ for the subsystem A.

In the semiclassical description, the (normalized) matter partition function $\mathbf{Z}_{\rm mat}$ computes the effective Rényi entropy of the quantum matter fields inside the entanglement wedge of $A \cup {\rm Is}(A)$ as follows

$$\frac{\mathbf{Z}_{\rm mat}[\mathcal{M}_n]}{\left(\mathbf{Z}_{\rm mat}[\mathcal{M}_1]\right)^n} = {\rm e}^{(1-n)\log {\rm Tr}\rho^n_{A\cup{\rm Is}(A)}}\,, \tag{3.21}$$

where $\rho_{A\cup{\rm Is}(A)}$ is the effective reduced density matrix in the semiclassical description.

Unlike the earlier works where JT gravity was coupled to a single radiation bath, in the current scenario, the presence of two baths modifies the structure of the dominant replica wormhole saddle to provide two independent mechanisms for the origin of the island region in the semiclassical description:

- For a subsystem $A = A^{\rm I} \cup A^{\rm II}$ with $A^{\rm I,II} \subset \mathcal{M}^{\rm I,II}$ in the radiation baths, both $A^{\rm I}$ and $A^{\rm II}$ are responsible for the conical singularities appearing in the gravitating manifold Σ. In this situation, the corresponding island region ${\rm Is}(A)$ manifested in Σ depends upon the degrees of freedom for both the CFT baths. In other words, if we denote the islands corresponding to the individual baths as ${\rm Is}^{\rm I,II}(A)$, for the present configuration we have ${\rm Is}^{\rm I}(A) = {\rm Is}^{\rm II}(A) \equiv {\rm Is}(A)$ and the density matrix in the effective theory factorizes in the following way

$$\rho_{A\cup{\rm Is}(A)} \sim \rho_{A^{\rm I}\cup{\rm Is}(A)} \otimes \rho_{A^{\rm II}\cup{\rm Is}(A)}\,. \tag{3.22}$$

JHEP11(2023)192

This could also be understood through the doubly holographic formalism where we have gravitational regions on either sides of the fluctuating EOW brane. Recall that in the doubly holographic description, the island region in this scenario is described by the region on the EOW brane between the two RTs crossing from AdS^{I} to AdS^{II}. For the present configuration the bulk RT surface homologous to the subsystem A is composed of two geodesics connecting the endpoints of A^{I} and A^{II}, each of which crosses the EOW brane only once as depicted in figure 4a. This corresponds to the conventional origin of the island region as described in [4, 5].

- On the other hand, consider a subsystem A residing entirely in the bath $\mathcal{M}^{\text{II}}$. If the central charge of the CFT^{II} is larger than that of the CFT^{I}, depending upon the size of the subsystem A, conical singularities in the gravitating region Σ may appear solely due to the presence of A in the bath $\mathcal{M}^{\text{II}}$. Since the bulk region Σ is common between the bath CFTs, the CFT^{I} degrees of freedom present in Σ sense the same conical singularities and conceive an *induced island* which we denote by $\text{Is}^{(\text{I}\setminus\text{II})}(A)$ to indicate that we obtain an island region in CFT^{I} given some subsystem A in CFT^{II}. In this case, the density matrix in the effective theory reduces to

$$\rho_{A\cup\text{Is}(A)} \sim \rho_{\text{Is}^{(\text{I}\setminus\text{II})}(A)} \otimes \rho_{A^{\text{II}}\cup\text{Is}(A)} \,. \tag{3.23}$$

  From the doubly holographic perspective, this corresponds to a double-crossing geodesic where the minimal curve penetrates into AdS^{I} and returns to AdS^{II} in order to satisfy the homology condition which is depicted in figure 4b. Note that such an island region is a novelty of the present model where a gravitational theory is coupled to two flat baths.

Assuming that the backreactions from the conical defects are small, the replica wormhole saddle are still solutions to the Einstein's equations. In such case, the classical gravitational action $\text{I}_{\text{grav}}[\Sigma_n]$ in eq. (3.20), for the replica wormhole saddle [4, 46] may be expressed for $n \sim 1$ as

$$\text{I}_{\text{grav}}[\Sigma_n] \approx n\, \text{I}_{\text{grav}}[\tilde{\Sigma}_1] + \frac{n-1}{4G_N^{(2)}} \mathcal{A}(\partial\text{Is}(A)) \,, \tag{3.24}$$

where $\tilde{\Sigma}_n \equiv \Sigma_n/\mathbb{Z}_n$ is the orbifold for the replicated bulk geometry Σ_n and $\mathcal{A}(\partial\text{Is}(A))$ is the area of the boundary of the island region $\text{Is}(A)$, namely the quantum extremal surface for the subsystem A. Utilizing eqs. (3.19), (3.20) and (3.24), we may now obtain the generalized entropy corresponding to the reduced density matrix $\boldsymbol{\rho}_A$ for the subsystem A as follows

$$\begin{aligned} S_{\text{gen}}\left(\boldsymbol{\rho}_A\right) &= \frac{\mathcal{A}(\partial\text{Is}(A))}{4G_N^{(2)}} + S_{\text{eff}}\left(\rho_{A\cup\text{Is}(A)}\right)_{\mathcal{M}^{\text{I}}\cup\mathcal{M}^{\text{II}}\cup\Sigma} \\ &= \frac{\mathcal{A}(\partial\text{Is}(A))}{4G_N^{(2)}} + S^{\text{I}}_{\text{eff}}\left(\rho_{A^{\text{I}}\cup\text{Is}(A)}\right)_{\mathcal{M}^{\text{I}}\cup\Sigma} + S^{\text{II}}_{\text{eff}}\left(\rho_{A^{\text{II}}\cup\text{Is}(A)}\right)_{\mathcal{M}^{\text{II}}\cup\Sigma} \,, \end{aligned} \tag{3.25}$$

for the conventional island. Note that the subscripts $\mathcal{M}^{\text{I,II}} \cup \Sigma$ denote that the reduced density matrices $\rho_{A^{\text{I,II}}\cup\text{Is}(A)}$ in the effective theory have support on corresponding manifolds. On the other hand, for the configuration where we observe the induced island, the

JHEP11(2023)192

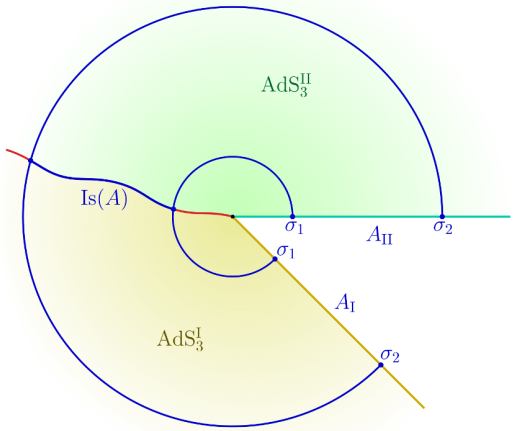

(a) Schematics of the bulk geodesic homologous to the subsystem $A = A_{\mathrm{I}} \cup A_{\mathrm{II}}$ described by a finite interval $A_{\mathrm{I,II}}$ in dual $\mathrm{CFT}^{\mathrm{I,II}}$.

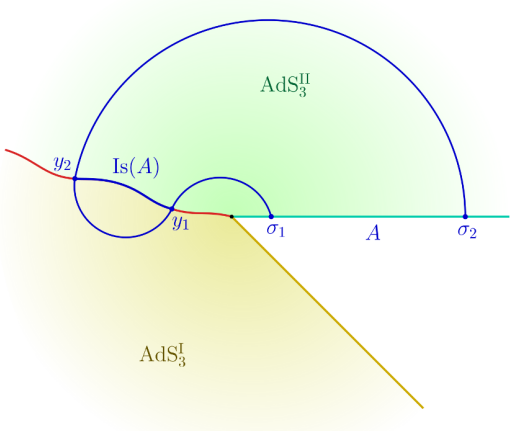

(b) Schematics of the (double-crossing) bulk geodesic homologous to the subsystem A described by a finite interval $[\sigma_1, \sigma_2]$ in dual $\mathrm{CFT}^{\mathrm{II}}$.

Figure 4. Two independent mechanisms for the origin of the island region $\mathrm{Is}(A)$ in ICFTs.

generalized entropy modifies to

$$S_{\mathrm{gen}}\left(\boldsymbol{\rho}_A\right) = \frac{\mathcal{A}\left(\partial \mathrm{Is}(A)\right)}{4G_N^{(2)}} + S_{\mathrm{eff}}^{\mathrm{I}}\left(\rho_{\mathrm{Is}^{(\mathrm{I}\setminus\mathrm{II})}(A)}\right)_{\Sigma} + S_{\mathrm{eff}}^{\mathrm{II}}\left(\rho_{A^{\mathrm{II}}\cup \mathrm{Is}(A)}\right)_{\mathcal{M}^{\mathrm{II}}\cup\Sigma}. \tag{3.26}$$

Note that the area term in eqs. (3.25) and (3.26) for the generalized entropies are as given in eq. (3.18).

4 Islands in extremal JT black holes

In this section, we will compute the entanglement entropies of various subsystems at a zero temperature in the $\mathrm{CFT}_2^{\mathrm{I}}$ and $\mathrm{CFT}_2^{\mathrm{II}}$ baths in the braneworld setup discussed above. In particular, we will compute the entanglement entropy for the corresponding subsystems in the intermediate picture using the island formula. Subsequently, we will substantiate these field theory results from the bulk computation of the RT surfaces corresponding to the subsystem using double holography in the large tension limit in which the gravity on the brane is weakly coupled.

As described in [3–5], the dilaton profiles may be obtained from the equation of motion which arises from the JT action in eq. (3.9) by varying it with respect to the metric for the case of extremal black hole as follows

$$\mathrm{d}s^2 = \frac{4\,\mathrm{d}\zeta_k \mathrm{d}\bar{\zeta}_k}{\left(\zeta_k + \bar{\zeta}_k\right)^2}, \qquad \Phi = \Phi_0 - \frac{2\Phi_r}{\zeta_k + \bar{\zeta}_k}, \tag{4.1}$$

where $\zeta = x + it_E$ are the planar coordinates and Φ_0 is the topological contribution to the dilaton given in eq. (3.18).

JHEP11(2023)192

4.1 Semi-infinite subsystem

We consider the case where a subsystem A is comprised of a semi-infinite interval in each bath CFT$_2$s as $A \equiv [\sigma_1, \infty]_{\rm I} \cup [\sigma_2, \infty]_{\rm II}$. We describe the computation of the entanglement entropy of the subsystem A using the island prescription in the effective $2d$ description discussed in section 3.1. Later we utilize the Ryu-Takayanagi (RT) prescription [47] to compute the entanglement entropy of the corresponding interval in the doubly holographic framework.

Effective $2d$ description. For this configuration involving a semi-infinite subsystem, only the conventional island appears. Consider the QES to be located at $-a$ on the EOW brane. Note that both the CFT$_2^{\rm I}$ and CFT$_2^{\rm II}$ are located on the JT brane, thus as discussed in section 3.1, the conical singularity at the QES $-a$ is present in both CFT$_2^{\rm I}$ and CFT$_2^{\rm II}$. As can be inferred from eq. (4.1), the UV cutoff on the JT brane has position dependence as $\epsilon(-a) = a$. Hence, utilizing eq. (3.25), the generalized entanglement entropy for subsystem A may be obtained as[11]

$$S_{\rm gen} = \frac{\Phi_r}{a} + \frac{c_{\rm I}}{6}\log\left[\frac{1}{\cos\psi_{\rm I}}\right] + \frac{c_{\rm II}}{6}\log\left[\frac{1}{\cos\psi_{\rm II}}\right] + \frac{c_{\rm I}}{6}\log\left[\frac{(\sigma_1+a)^2}{\epsilon\, a}\right] + \frac{c_{\rm II}}{6}\log\left[\frac{(\sigma_2+a)^2}{\epsilon\, a}\right], \tag{4.2}$$

where we have used eq. (3.18) for the area of the quantum extremal surface located on the JT brane. The entanglement entropy may now be obtained through the extremization of the above generalized entropy over the position of the island surface. The extremization for arbitrary σ_1 and σ_2, however leads to complicated expressions. Thus for simplicity, we assume the symmetric case $\sigma_1 = \sigma_2 = \sigma$, for which the extremization equation is given by

$$\partial_a S_{\rm gen} = 0 \quad \Rightarrow \qquad a\,(c_{\rm I}+c_{\rm II})\,(a-\sigma) - 6(a+\sigma)\Phi_r \;= 0\,. \tag{4.3}$$

Finally, the location of the island region a^* may be obtained from the above quadratic equation as follows

$$a^* = \frac{(c_{\rm I}+c_{\rm II})\,\sigma + 6\Phi_r + \sqrt{\left((c_{\rm I}+c_{\rm II})\,\sigma + 6\Phi_r\right)^2 + 24\,(c_{\rm I}+c_{\rm II})\,\sigma\Phi_r}}{2\,(c_{\rm I}+c_{\rm II})}\,, \tag{4.4}$$

where we have disregarded the unphysical solution of the QES. The fine-grained entropy for the subsystem A may finally be obtained by substituting the above extremal value in eq. (4.2). In order to compare this result with the doubly holographic computation in the following subsection, we need to consider the large tension limit of the JT brane for which the brane angles $\psi_{\rm I,II}$ may be expanded as [39]

$$\psi_{\rm I} = \frac{\pi}{2} - \frac{L_{\rm I}}{L_{\rm I}+L_{\rm II}}\delta\,, \qquad \psi_{\rm II} = \frac{\pi}{2} - \frac{L_{\rm II}}{L_{\rm I}+L_{\rm II}}\delta\,, \qquad \text{with } \delta \to 0\,, \tag{4.5}$$

where the finite but small δ describes the deviation of the JT brane from the extended conformal boundary of the AdS$_3^{\rm I,II}$.

[11] In the following we will set $4G_N^{(2)} = 1$ for brevity.

JHEP11(2023)192

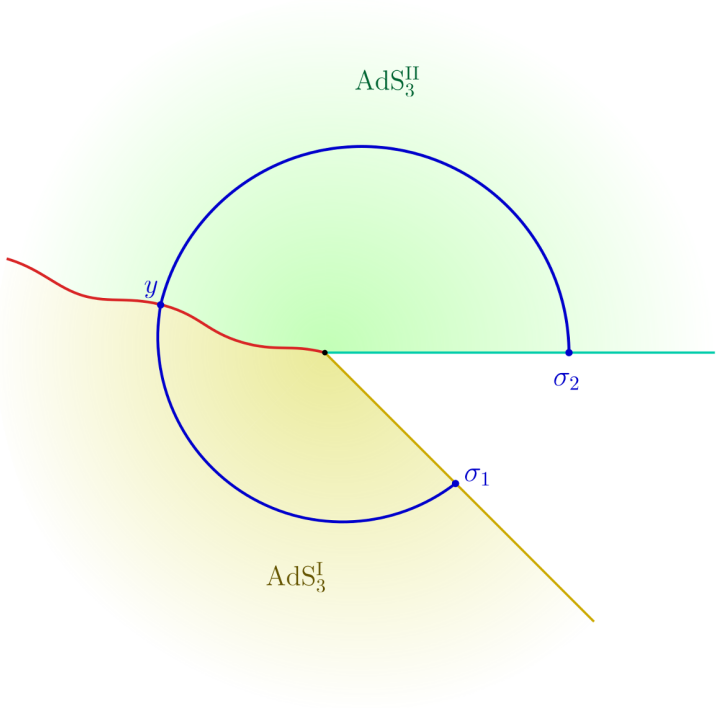

Figure 5. Schematics of the bulk geodesic homologous to the subsystem A described by the union of two semi-infinite intervals in both $\mathrm{CFT}^{\mathrm{I}}$ and $\mathrm{CFT}^{\mathrm{II}}$.

Doubly holographic description. In this subsection, we substantiate the above island results in the effective field theory from a doubly holographic perspective. To this end, the metric described in eq. (2.12) may be mapped to the Poincaré AdS_3 geometry through the following coordinate transformations

$$z_k = y\cos\chi_k\,, \qquad x_k = y\sin\chi_k. \tag{4.6}$$

The radial direction in the xz-plane in the Poincaré coordinates is described by the coordinate y. At the asymptotic boundary described by $\chi_k = \pm\pi/2$, y now serves as a boundary coordinate. Furthermore, the length of a geodesic between points (t, x, z) and (t', x', z') in the Poincaré coordinates, is obtained through

$$d = L\,\cosh^{-1}\left[\frac{-(t-t')^2+(x-x')^2+z^2+z'^2}{2z\,z'}\right]. \tag{4.7}$$

Note that for the present configuration, the RT surface homologous to subsystem A consists of two semi-circular geodesic segments in each of the $\mathrm{AdS}_3^{\mathrm{I,II}}$ geometries which are smoothly joined at the EOW brane as depicted in figure 5. As a consequence of the Israel junction condition, we may choose the common point on the EOW brane to be parametrized by a single variable y. The total length of the RT surface may then be expressed as

$$d = L_{\mathrm{I}}\log\left[\frac{(\sigma_1+y\sin\psi_{\mathrm{I}})^{\,2}+(y\cos\psi_{\mathrm{I}})^2}{\epsilon\,y\cos\psi_{\mathrm{I}}}\right]+L_{\mathrm{II}}\log\left[\frac{(\sigma_2+y\sin\psi_{\mathrm{II}})^2+(y\cos\psi_{\mathrm{II}})^2}{\epsilon\,y\cos\psi_{\mathrm{II}}}\right], \tag{4.8}$$

JHEP11(2023)192

Subsequently, we perturb the EOW brane by introducing a small fluctuation in the brane angles $\psi_{\rm I,II}$ as follows

$$\psi_k(y) \to \sin^{-1}\left[\tanh\left(\frac{\rho_k^0+(-1)^k\tilde{\rho}_k(y)}{L_k}\right)\right], \tag{4.9}$$

where $\frac{\tilde{\rho}_{\rm I,II}}{\rho^0_{\rm I,II}} \ll 1$. Utilizing the above relation, eq. (4.8) reduces to

$$\begin{aligned} d = L_{\rm I}\log\left[\frac{2\sigma_1 y\tanh\left(\frac{\rho_{\rm I}^0}{L_{\rm I}}\right)+\sigma_1^2+y^2}{\epsilon\, y\,\mathrm{sech}\left(\frac{\rho_{\rm I}^0}{L_{\rm I}}\right)}\right]+L_{\rm II}\log\left[\frac{2\sigma_2 y\tanh\left(\frac{\rho_{\rm II}^0}{L_{\rm II}}\right)+\sigma_2^2+y^2}{\epsilon\, y\,\mathrm{sech}\left(\frac{\rho_{\rm II}^0}{L_{\rm II}}\right)}\right] \\ -\frac{\tilde{\rho}_{\rm I}\left(\sigma_1^2\tanh\left(\frac{\rho_{\rm I}^0}{L_{\rm I}}\right)+y^2\tanh\left(\frac{\rho_{\rm I}^0}{L_{\rm I}}\right)+2\sigma_1 y\right)}{2\sigma_1 y\tanh\left(\frac{\rho_{\rm I}^0}{L_{\rm I}}\right)+\sigma_1^2+y^2}+\frac{\tilde{\rho}_{\rm II}\left(\sigma_2^2\tanh\left(\frac{\rho_{\rm II}^0}{L_{\rm II}}\right)+y^2\tanh\left(\frac{\rho_{\rm II}^0}{L_{\rm II}}\right)+2\sigma_2 y\right)}{2\sigma_2 y\tanh\left(\frac{\rho_{\rm II}^0}{L_{\rm II}}\right)+\sigma_2^2+y^2}. \end{aligned} \tag{4.10}$$

where we have considered terms up to the first order in $\tilde{\rho}_{\rm I,II}$. Note that, the perturbative parameters $\tilde{\rho}_{\rm I,II}$ are functions of the island location y. Therefore, in the perturbative terms of the above expression, we replace y with its zeroth order solution in $\tilde{\rho}_{\rm I,II}$ such that the geodesic length in eq. (4.10) contains terms truly upto the first order in $\tilde{\rho}_{\rm I,II}$. Subsequently, on identifying the dilaton as given in eq. (3.12), the candidate entanglement entropy may be obtained as follows

$$S_{\rm single}(\sigma,y) = \frac{\Phi_r}{y}+\frac{L_{\rm I}}{4G_N}\log\left[\frac{\sigma^2+y^2+2\sigma\, y\sin\psi_{\rm I}}{\epsilon\, y\cos\psi_{\rm I}}\right]+\frac{L_{\rm II}}{4G_N}\log\left[\frac{\sigma^2+y^2+2\sigma\, y\sin\psi_{\rm II}}{\epsilon\, y\cos\psi_{\rm II}}\right], \tag{4.11}$$

where we have considered $\sigma_1 = \sigma_2 = \sigma$ for simplicity. Now, to obtain the holographic entanglement entropy, we extremize the above with respect to y to obtain

$$\begin{aligned} L_{\rm II}\, y(y-\sigma)(y+\sigma)\left[\left(y^2+\sigma^2\right)\left(\cos\psi_{\rm I}\,\sec\psi_{\rm II}+1\right)+2\sigma\, y\sin(\psi_{\rm I}+\psi_{\rm II})\sec\psi_{\rm II}\right] \\ -4G_N\Phi_r\left(y^2+\sigma^2+2\sigma\, y\sin\psi_{\rm I}\right)\left(y^2+\sigma^2+2\sigma\, y\sin\psi_{\rm II}\right)=0. \end{aligned} \tag{4.12}$$

The entanglement entropy for the semi-infinite subsystem in question may be obtained by substituting the physical solution for y in eq. (4.11). Finally, in the large tension limit described in eq. (4.5), this matches exactly with the corresponding entanglement entropy computed in the effective $2d$ theory on utilization of the Brown-Henneaux formula $c_{\rm I,II} = \frac{3L_{\rm I,II}}{2G_N}$ [48].

4.2 Finite subsystem

In this subsection, we obtain the entanglement entropy for a finite sized subsystem $A \equiv [\sigma_1,\sigma_2]_{\rm I}\cup[\sigma_1,\sigma_2]_{\rm II}$ located in the baths $\mathrm{CFT}_2^{\rm I}$ and $\mathrm{CFT}_2^{\rm II}$. Here, we observe three non-trivial phases for the generalized entanglement entropy depending upon the sizes of the subsystem A as depicted in figures 6 to 8 . In this context, we first utilize the effective

JHEP11(2023)192

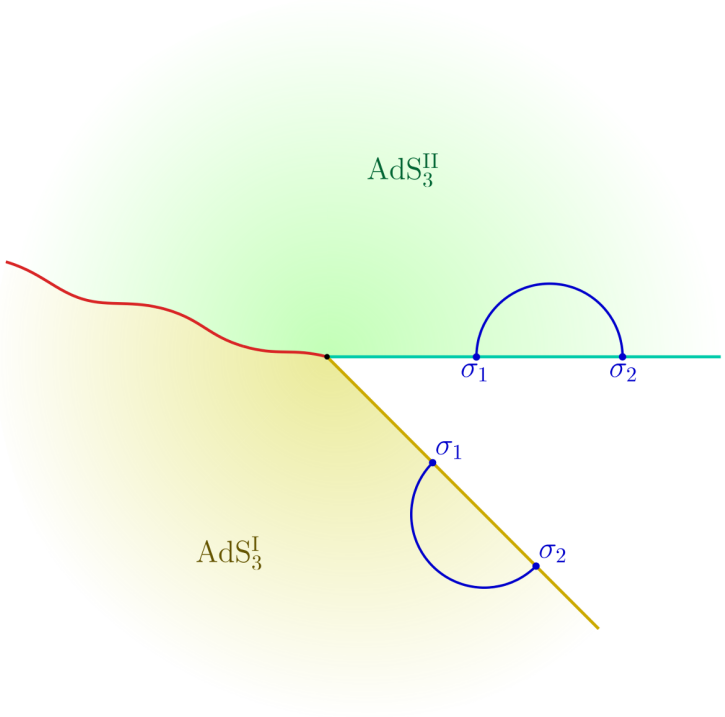

Figure 6. Schematics of the phase-I for the bulk geodesic homologous to the subsystem A described by a finite interval $[\sigma_1, \sigma_2]_{\mathrm{I,II}}$ in dual $\mathrm{CFT}^{\mathrm{I,II}}$.

$2d$ prescription to compute the generalized entanglement entropy for the corresponding subsystem in these scenarios. Subsequently, we provide a doubly holographic characterization of the entanglement entropy for the three cases using the RT prescription which substantiates the corresponding field theory results.

4.2.1 Phase - I

Effective 2*d* description. We begin with the computation of the generalized entanglement entropy for the phase where the intervals $[\sigma_1, \sigma_2]_{\mathrm{I}}$ and $[\sigma_1, \sigma_2]_{\mathrm{II}}$ are small such that no island region is observed as depicted in figure 6. For this configuration the area term in generalized entropy vanishes and the expression for the entanglement entropy may trivially be obtained to be

$$S_A = \frac{(c_{\mathrm{I}} + c_{\mathrm{II}})}{3} \log\left[\frac{\sigma_2 - \sigma_1}{\epsilon}\right] . \tag{4.13}$$

Doubly holographic description. From the doubly holographic perspective, it may be observed that the RT surfaces for the intervals $[\sigma_1, \sigma_2]_{\mathrm{I,II}}$ in $\mathrm{CFT}_2^{\mathrm{I,II}}$ are described by the usual dome-shaped geodesics each in the dual bulk $\mathrm{AdS}_3^{\mathrm{I,II}}$ geometries as depicted in figure 6. The entanglement entropy for this configuration may then be obtained to be

$$S_{\mathrm{dome}} = \frac{(L_{\mathrm{I}} + L_{\mathrm{II}})}{4G_N} \log\left[\frac{\sigma_2 - \sigma_1}{\epsilon}\right] , \tag{4.14}$$

JHEP11(2023)192

which matches identically with the corresponding expression obtained in the effective $2d$ description in eq. (4.13) through the utilization of the Brown-Henneaux formula.

4.2.2 Phase - II

Effective $2d$ description. We now discuss the next phase where the sizes of the intervals in the $\text{CFT}_{\text{I,II}}$ are increased such that we now observe an island region on the JT brane described by $[-a_2, -a_1]_{\text{I,II}}$. Note that this configuration corresponds to the conventional origin of the island as discussed in section 3.1. The effective terms of the generalized entanglement entropy given in eq. (3.25) for this case may be obtained through the four-point twist correlators in $\text{CFT}_2^{\text{I,II}}$ which factorize in the large-c limit in the following way

$$\left\langle \mathcal{T}_n(\sigma_1)\bar{\mathcal{T}}_n(\sigma_2)\mathcal{T}_n(-a_2)\bar{\mathcal{T}}_n(-a_1)\right\rangle_{\text{CFT}_2^k} = \left\langle \mathcal{T}_n(\sigma_1)\bar{\mathcal{T}}_n(-a_1)\right\rangle_{\text{CFT}_2^k}\left\langle \bar{\mathcal{T}}_n(\sigma_2)\mathcal{T}_n(-a_2)\right\rangle_{\text{CFT}_2^k} . \tag{4.15}$$

Subsequently, we may express the generalized entropy in the large-tension limit as follows,

$$\begin{aligned} S_{\text{gen}} = &\frac{\Phi_r}{a_1} + \frac{c_{\text{I}}}{6}\log\left[\left(\frac{L_{\text{I}}+L_{\text{II}}}{L_{\text{I}}\,\delta}\right)\frac{(\sigma_1+a_1)^2}{a_1}\right] + \frac{c_{\text{II}}}{6}\log\left[\left(\frac{L_{\text{I}}+L_{\text{II}}}{L_{\text{II}}\,\delta}\right)\frac{(\sigma_1+a_1)^2}{a_1}\right] \\ &+ \frac{\Phi_r}{a_2} + \frac{c_{\text{I}}}{6}\log\left[\left(\frac{L_{\text{I}}+L_{\text{II}}}{L_{\text{I}}\,\delta}\right)\frac{(\sigma_2+a_2)^2}{a_2}\right] + \frac{c_{\text{II}}}{6}\log\left[\left(\frac{L_{\text{I}}+L_{\text{II}}}{L_{\text{II}}\,\delta}\right)\frac{(\sigma_2+a_2)^2}{a_2}\right] . \end{aligned} \tag{4.16}$$

Similar to section 4.1, the above may be extremized over the positions of the QES at a_1 and a_2 to obtain expressions similar to eq. (4.4) with σ replaced by σ_1 and σ_2 respectively. Finally, the entanglement entropy for this configuration may be obtained by substituting these extremal values of the island locations in the above generalized entropy.

Doubly holographic description. For this phase, owing to the conventional island, the RT surface homologous to subsystem A is composed of two single-crossing geodesics of the type discussed in section 4.1 and as depicted in figure 7. Consequently, the candidate entanglement entropy for the present configuration may be expressed as

$$S_{\text{bulk}} = S_{\text{single}}(\sigma_1, y_1) + S_{\text{single}}(\sigma_2, y_2) . \tag{4.17}$$

As earlier, to obtain the locations of the common points y_is on the EOW brane, we extremize the above with respect to y_1 and y_2 to obtain equations analogous to eq. (4.12) whose physical solutions will lead to the holographic entanglement entropy. Subsequently in the large tension limit described by eq. (4.5), this agrees with the corresponding result in the effective $2d$ description.

4.2.3 Phase - III

Effective $2d$ description. We now proceed to the final phase depicted in figure 8 which involves the novel induced islands discussed in section 3.1. The location of this island region is described by $[a_1, a_2]_{\text{I,II}}$ on the JT brane for the given subsystem. For this phase, we utilize the generalized entanglement entropy formula in eq. (3.26) for the corresponding subsystem A. The presence of induced island results in the factorization of the four-point

JHEP11(2023)192

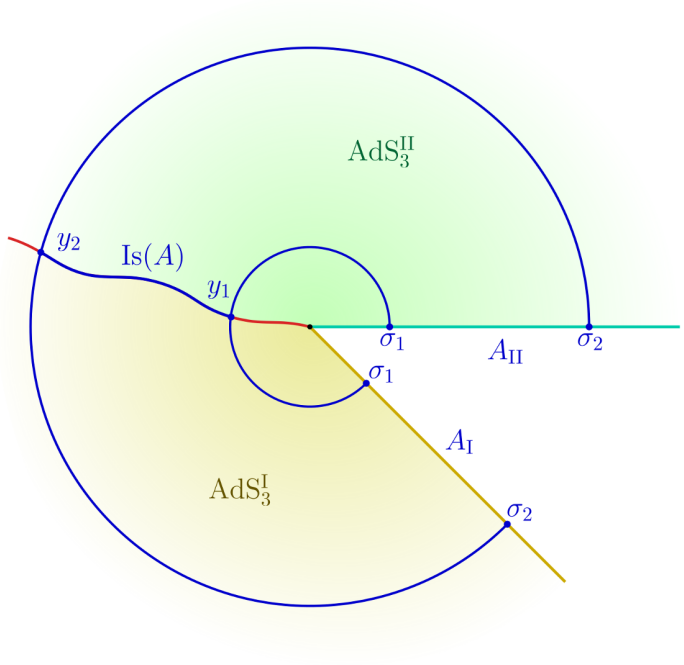

Figure 7. Schematics of the phase-II for the bulk geodesic homologous to the subsystem A described by a finite interval $[\sigma_1, \sigma_2]_{\mathrm{I,II}}$ in dual $\mathrm{CFT}^{\mathrm{I,II}}$. Here $\mathrm{Is}(A)$ denotes the island region in the effective $2d$ description.

twist correlators in the effective terms of the generalized entanglement entropy in the following way

$$\begin{aligned}\left\langle \mathcal{T}_n(\sigma_1)\bar{\mathcal{T}}_n(\sigma_2)\mathcal{T}_n(-a_2)\bar{\mathcal{T}}_n(-a_1)\right\rangle_{\mathrm{CFT}_2^{\mathrm{I}}} &= \left\langle \mathcal{T}_n(\sigma_1)\bar{\mathcal{T}}_n(\sigma_2)\right\rangle_{\mathrm{CFT}_2^{\mathrm{I}}}\left\langle \mathcal{T}_n(-a_1)\bar{\mathcal{T}}_n(-a_2)\right\rangle_{\mathrm{CFT}_2^{\mathrm{I}}}\\ \left\langle \mathcal{T}_n(\sigma_1)\bar{\mathcal{T}}_n(\sigma_2)\mathcal{T}_n(-a_2)\bar{\mathcal{T}}_n(-a_1)\right\rangle_{\mathrm{CFT}_2^{\mathrm{II}}} &= \left\langle \mathcal{T}_n(\sigma_1)\bar{\mathcal{T}}_n(-a_1)\right\rangle_{\mathrm{CFT}_2^{\mathrm{II}}}\left\langle \mathcal{T}_n(\sigma_2)\bar{\mathcal{T}}_n(-a_2)\right\rangle_{\mathrm{CFT}_2^{\mathrm{II}}}.\end{aligned} \tag{4.18}$$

On utilization of the area term given in eq. (3.18) and the position dependent cut-off $\epsilon(y)$ on the JT brane, the generalized entanglement entropy in this case may then be expressed as

$$\begin{aligned}S_{\mathrm{gen}} = \frac{\Phi_r}{a_1} + \frac{\Phi_r}{a_2} + \frac{c_{\mathrm{I}}}{3}\log\left[\frac{1}{\cos\psi_{\mathrm{I}}}\right] + \frac{c_{\mathrm{II}}}{3}\log\left[\frac{1}{\cos\psi_{\mathrm{II}}}\right] + \frac{c_{\mathrm{I}}}{6}\log\left[\frac{(\sigma_2-\sigma_1)}{\epsilon}\right]\\ + \frac{c_{\mathrm{I}}}{6}\log\left[\frac{(a_1-a_2)^2}{a_1\,a_2}\right] + \frac{c_{\mathrm{II}}}{6}\log\left[\frac{(\sigma_1+a_1)^2}{\epsilon\,a_1}\right] + \frac{c_{\mathrm{II}}}{6}\log\left[\frac{(\sigma_2+a_2)^2}{\epsilon\,a_2}\right].\end{aligned} \tag{4.19}$$

We now introduce a parameter $\Theta = \frac{\sigma_2}{\sigma_1}$ which is motivated from the analysis[12] described in [39]. Moreover, one can also establish a similar relation between the QES a_1 and a_2 located on the JT brane as $a_2 = \kappa\,\Theta\,a_1$ where κ is now one of the parameters whose extremal value will minimize the entanglement entropy. In the case of non-perturbed EOW brane where we obtain the usual ICFT_2 setup, it was shown in [39] that the current phase is

[12]Note that the authors [39] only described the bulk computation of the entanglement entropy for finite interval located in the $\mathrm{CFT}_2^{\mathrm{II}}$.

JHEP11(2023)192

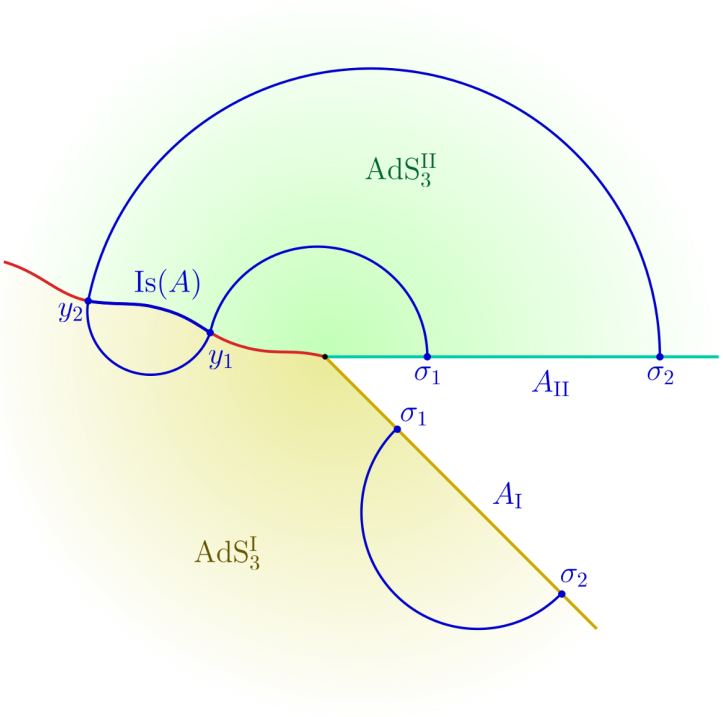

Figure 8. Schematics of the phase-III for the bulk geodesic homologous to the subsystem A described by the finite interval $[\sigma_1, \sigma_2]_{\rm I,II}$ in dual CFT$^{\rm I,II}$. Here Is(A) denotes the *induced* island region in the effective $2d$ description.

only possible above a certain value of the parameter Θ depending upon the configuration of the EOW brane. Thus in our computations we assume Θ to be large. Finally, we introduce Θ and κ in eq. (4.19), and extremize over the parameters a_1 and κ in the large tension limit to obtain the following relations,

$$\begin{aligned} \partial_\kappa S_{\rm gen} = 0 \quad &\Rightarrow \quad a_1\,(c_{\rm I}+c_{\rm II})\,\kappa + (c_{\rm I}-c_{\rm II})\,\sigma_1 = 0 \\ \partial_{a_1} S_{\rm gen} = 0 \quad &\Rightarrow \quad a_1\sigma_1\,(c_{\rm II}\sigma_1 + 3(\kappa+1)\Phi_r) - a_1^3\kappa\,c_{\rm II} + 3a_1^2\kappa\,\Phi_r + 3\sigma_1^2\Phi_r = 0\,. \end{aligned} \tag{4.20}$$

Solving the above, the extremal values of the QES are obtained to be

$$\begin{aligned} \kappa^* &= \frac{(c_{\rm II}-c_{\rm I})\;\sigma_1}{(c_{\rm I}+c_{\rm II})\;a_1^*} \\ a_1^* &= \frac{(c_{\rm I}+c_{\rm II})\,\sigma_1 + 6\Phi_r + \sqrt{\left((c_{\rm I}+c_{\rm II})\,\sigma_1 + 6\Phi_r\right)^2 + 24\,(c_{\rm II}-c_{\rm I})\,\sigma_1\Phi_r}}{2\,(c_{\rm II}-c_{\rm I})} \end{aligned} \tag{4.21}$$

where we have only considered the physical solutions of the island surfaces. The fine grained entropy for the subsystem A may now be obtained by substituting the above extremal value in the generalized entropy in eq. (4.19).

Doubly holographic description. In this subsection we obtain the length of the RT surfaces supported by the finite-sized subsystem $[\sigma_1, \sigma_2]_{\rm I,II}$ located in the dual CFT$_2^{\rm I,II}$ as

JHEP11(2023)192

depicted in figure 8. The interval in CFT_2^{I} supports the usual boundary anchored dome-shaped geodesic. However, for the interval in CFT_2^{II}, the extremal curve is composed of three circular segments forming a double-crossing RT saddle as discussed in section 3.1. This double-crossing geodesic intersects the EOW brane at y_1 and y_2 which form the boundary of the island region in the effective $2d$ description.

Utilizing eq. (4.7), the length of the double-crossing geodesic may be obtained as[13]

$$\begin{aligned} d = L_{\text{I}} \cosh^{-1}\left[\frac{(y_2-y_1)^2 \sin\psi_{\text{I}}(y_1)\sin\psi_{\text{I}}(y_2) + (y_1^2+y_2^2)\cos\psi_{\text{I}}(y_1)\cos\psi_{\text{I}}(y_2)}{2y_1y_2\cos\psi_{\text{I}}(y_1)\cos\psi_{\text{I}}(y_2)}\right] \\ + L_{\text{II}}\log\left[\frac{(\sigma_1+y_1\sin\psi_{\text{II}}(y_1))^2+(y_1\cos\psi_{\text{II}}(y_1))^2}{y_2\cos\psi_{\text{II}}(y_1)}\right] \\ + L_{\text{II}}\log\left[\frac{(\sigma_2+y_2\sin\psi_{\text{II}}(y_2))^2+(y_2\cos\psi_{\text{II}}(y_2))^2}{y_2\cos\psi_{\text{II}}(y_2)}\right]. \end{aligned} \tag{4.22}$$

We may now introduce the variables $\Theta = \frac{\sigma_2}{\sigma_1}$ and $y_2 = \hat{\kappa}\,\Theta\, y_1$, similar to the effective $2d$ perspective considered earlier. As advocated in [39] in the context of $\text{AdS}_3/\text{ICFT}_2$, such double-crossing geodesics are only permissible for large Θs. Consequently, in the large Θ limit of the above length, we obtain

$$\begin{aligned} d \approx L_{\text{I}}\log\left[\frac{\Theta\,\hat{\kappa}}{\cos\psi_{\text{I}}(y_1)\cos\psi_{\text{I}}(y_2)}\right] + L_{\text{II}}\log\left[\frac{\sigma_1^2+2y_1\sigma_1\sin\psi_{\text{II}}(y_1)+y_1^2}{y_1\cos\psi_{\text{II}}(y_1)}\right] \\ + L_{\text{II}}\log\left[\frac{\Theta(\sigma_1^2+2\hat{\kappa}y_1\sigma_1\sin\psi_{\text{II}}(y_2)+\hat{\kappa}^2y_1^2)}{\hat{\kappa}\,y_1\cos\psi_{\text{II}}(y_2)}\right]. \end{aligned} \tag{4.23}$$

Next we implement the position dependence of the brane angles $\psi_{\text{I,II}}(y_i)$ explicitly in the following way

$$\begin{aligned} \psi_{\text{I}}(y_i) &\to \sin^{-1}\left[\tanh\left(\frac{\rho_{\text{I}}^0-\tilde{\rho}_{\text{I}}(y_i)}{L_{\text{I}}}\right)\right], \\ \psi_{\text{II}}(y_i) &\to \sin^{-1}\left[\tanh\left(\frac{\rho_{\text{II}}^0+\tilde{\rho}_{\text{II}}(y_i)}{L_{\text{II}}}\right)\right]. \end{aligned} \tag{4.24}$$

Expanding eq. (4.23) upto the leading order in $\tilde{\rho}_{\text{I,II}}$ and identifying the dilaton as in eq. (3.12), we may obtain the corresponding contribution from the double-crossing geodesic as follows

$$\begin{aligned} S_{\text{double}}(y_1,y_2) = \frac{\Phi_r}{y_2}+\frac{\Phi_r}{y_1}+\frac{L_{\text{I}}}{4G_N}\log\left[\frac{y_2}{y_1}\sec^2(\psi_{\text{I}})\right] \\ + \frac{L_{\text{II}}}{4G_N}\log\left[\frac{(\sigma_2^2+2y_2\,\sigma_2\sin\psi_{\text{II}}+y_2^2)\,(\sigma_1^2+2y_1\,\sigma_1\sin\psi_{\text{II}}+y_1^2)}{y_1\,y_2\cos^2\psi_{\text{II}}}\right], \end{aligned} \tag{4.25}$$

where we have restored the original variables σ_2 and y_2.

[13] Note that the transverse fluctuation of the EOW brane requires the brane angles $\psi_{\text{I,II}}(y_i)$ to be position dependent.

JHEP11(2023)192

Finally the candidate entanglement entropy for finite sized subsystem under consideration may be obtained by including the contribution from the dome-shaped geodesic as follows

$$S_{\text{bulk}} = S_{\text{double}}(y_1, y_2) + \frac{L_{\text{I}}}{4G_N} \log\left[\frac{(\sigma_2 - \sigma_1)}{\epsilon}\right] . \tag{4.26}$$

The above may be extremized over the undetermined parameters y_1 and y_2 to obtain

$$\begin{aligned} 2y_1\,\sigma_1 \sin\psi_{\text{II}}\,(4G_N\Phi_r \sin\psi_{\text{I}} + L_{\text{I}} y_1) + \sigma_1^2\,(4G_N\Phi_r \sin(\psi_{\text{I}}) + (L_{\text{I}} + L_{\text{II}})\,y_1) \\ - y_1^2\,((L_{\text{II}} - L_{\text{I}})\,y_1 - 4G_N\Phi_r \sin\psi_{\text{I}}) = 0\,, \end{aligned} \tag{4.27}$$

$$\begin{aligned} 2y_2\,\sigma_2 \sin\psi_{\text{II}}\,(4G_N\Phi_r \sin\psi_{\text{I}} - L_{\text{I}} y_2) + \sigma_2^2\,(4G_N\Phi_r \sin\psi_{\text{I}} - (L_{\text{I}} - L_{\text{II}})\,y_2) \\ - y_2^2\,((L_{\text{I}} + L_{\text{II}})\,y_2 - 4G_N\Phi_r \sin\psi_{\text{I}}) = 0. \end{aligned} \tag{4.28}$$

Solving the above equations for y_1 and y_2 and substituting the extremal values in eq. (4.26) will finally result in the holographic entanglement entropy for the given finite subsystem. Once again, in the large tension limit described in eq. (4.5), we observe that the corresponding entanglement entropy obtained through the effective $2d$ description is reproduced.

4.2.4 Page curve

We now plot the entanglement entropy for the finite subsystem A under consideration in the dual $\text{CFT}_2^{\text{I,II}}$s with respect to the variable $\Theta = \frac{\sigma_2}{\sigma_1}$ parameterizing the subsystem size in figure 9. For the given value of parameters, we observe transitions between the three phases discussed above as the subsystem size is increased. Initially when the subsystem is small in size, phase-I has the minimum entanglement entropy and is dominant. As we increase the subsystem size, subsequently phase-III starts dominating as crossing over to the region with smaller AdS radius AdS_3^{I}, is more economical for the geodesic. Finally if the subsystem size is further increased, this advantage of double-crossing vanishes as the length of dome-shaped RT surface supported by the interval in CFT_2^{I} keeps increasing. And ultimately, phase-II becomes dominant.

5 Islands outside eternal JT black holes

In this section, we consider semi-infinite subsystems in thermal CFT_2 baths coupled to an eternal JT black hole. The thermofield double (TFD) state in this case may be constructed through the Euclidean path integral on half of an infinite cylinder [39]. The corresponding cylinder geometry may be obtained by applying a series of transformations on the planar ICFT_2 setup described by $\zeta = x + it_E$. We begin by mapping the flat interface to a circle of length ℓ through the following $\text{SL}(2,\mathbb{R})$ transformation

$$p = \frac{4\ell^2}{2\ell - \zeta} - \ell\,, \tag{5.1}$$

where $p = \tilde{x} + i\tilde{t}_E$. The corresponding bulk transformations may be obtained through the Bañados formalism [49–51] as follows

$$\tilde{x} = \frac{x - \frac{x^2+z^2-t^2}{2\ell}}{1 - \frac{x}{\ell} + \frac{x^2+z^2-t^2}{4\ell^2}} + \ell\,, \qquad \tilde{z} = \frac{z}{1 - \frac{x}{\ell} + \frac{x^2+z^2-t^2}{4\ell^2}}\,, \qquad \tilde{t} = \frac{t}{1 - \frac{x}{\ell} + \frac{x^2+z^2-t^2}{4\ell^2}}\,. \tag{5.2}$$

JHEP11(2023)192

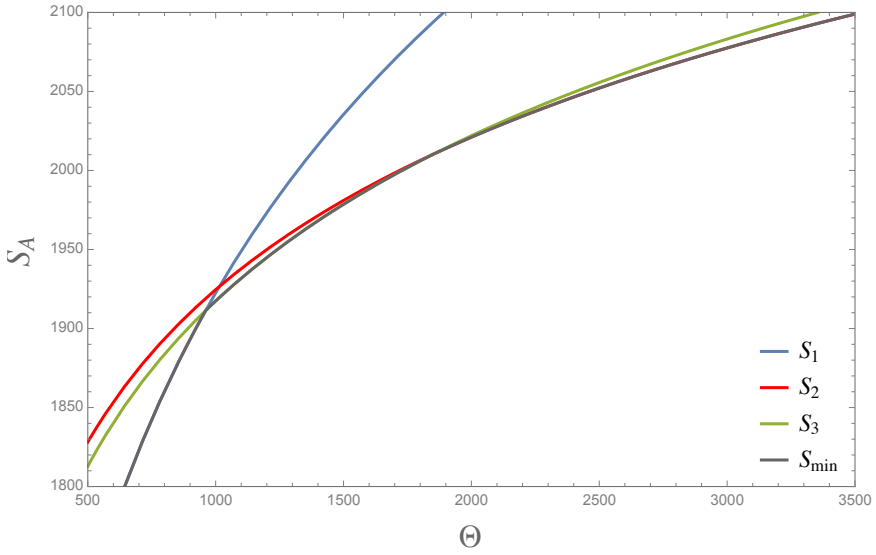

Figure 9. Variation of the entanglement entropy with $\Theta = \frac{\sigma_2}{\sigma_1}$ for the finite sized subsystem A where $c_{\rm I} = 35, c_{\rm II} = 800, \Phi_r = 6.958, \delta = 0.1, \sigma_1 = 0.4$. Here S_1, S_2, S_3 correspond to the entropy in phase-I, phase-II and phase-III respectively. The entanglement entropy is given by the minimum $S_{\rm min}$ of these possible candidates for a given subsystem size.

We further obtain the cylinder geometry via the usual exponential map given by

$$p = \ell e^{\frac{2\pi}{\beta} q}\,, \tag{5.3}$$

where the coordinate $q = u + iv_E$ describes the cylinder with circumference β. The interface is now mapped to a circle $\mathfrak{Re}(q) = 0$ with the two CFT$_2$s mapped on either side. The dual bulk theory for the TFD state on this cylinder is then described by an eternal black string spanning two AdS$_3$ geometries separated by a thin AdS$_2$ brane. The horizon of the black string crosses the brane and induces a horizon on it. A similar partial dimensional reduction as described in section 3 may now be performed for this $3d$ bulk to obtain an effective $2d$ description comprising of two thermal CFT$_2$ baths coupled to an eternal JT black hole.

In the cylinder coordinates, the metric and the dilaton profile for the eternal JT black hole in AdS$_2$ are given as follows [3–5]

$$\mathrm{d}s^2_{\rm grav} = \frac{4\pi^2}{\beta^2}\frac{\mathrm{d}q\,\mathrm{d}\bar{q}}{\sinh^2\left(\frac{\pi(q+\bar{q})}{\beta}\right)}\,, \qquad \Phi = \Phi_0 - \frac{2\pi\Phi_r}{\beta}\coth\left(\frac{\pi(q+\bar{q})}{\beta}\right)\,, \tag{5.4}$$

where Φ_0 is the topological contribution to the dilaton given in eq. (3.18). On the other hand, the metric for the CFT$_2$ baths may be expressed as

$$\mathrm{d}s^2_{\rm bath} = \frac{1}{\epsilon^2}\mathrm{d}q\,\mathrm{d}\bar{q}\,. \tag{5.5}$$

However, in the following we will employ the planar coordinates p in which the field theory remains in the ground state and the corresponding stress tensor vanishes. The

JHEP11(2023)192

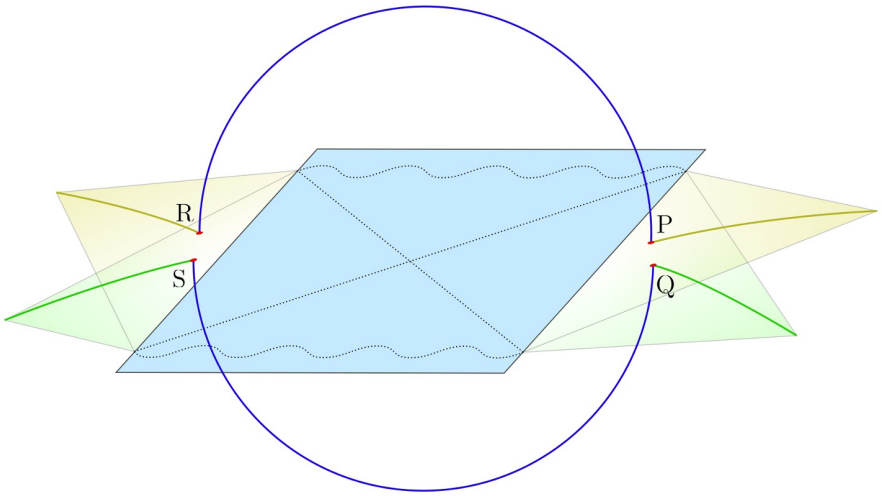

Figure 10. Schematics for the semi-infinite subsystem A in phase-I where the extremal curve is composed of two Hartman-Maldacena surfaces.

corresponding metrics and the dilaton are given as follows

$$\mathrm{d}s^2_{\text{grav}} = \frac{4}{(1-|p|^2)^2}\mathrm{d}p\,\mathrm{d}\bar{p}, \qquad \mathrm{d}s^2_{\text{bath}} = \frac{\beta^2}{4\pi^2\epsilon^2}\frac{\mathrm{d}p\,\mathrm{d}\bar{p}}{|p|^2}\,,$$
$$\Phi = \Phi_0 + \frac{2\pi\Phi_r}{\beta}\frac{1+|p|^2}{1-|p|^2}\,. \tag{5.6}$$

We will now obtain the fine-grained entanglement entropy for a semi-infinite subsystem in bath $\text{CFT}_2^{\text{I,II}}$s coupled to an eternal JT black hole. For this case, we observe two phases for the entanglement entropy as depicted in figures 10 and 11. Specifically, for the first phase, we do not observe islands and obtain a steadily rising entanglement entropy as the black hole evolves. For the second phase, QES are observed outside the eternal JT black holes, indicating the presence of islands which saturates the entanglement entropy.

5.1 Phase - I

Effective 2*d* description. Now we describe the computation of the generalized entanglement entropy in the first phase for the subsystem composed of semi-infinite intervals $[P,\infty]_{\text{I}} \cup [R,\infty]_{\text{I}}$ considered in CFT_2^{I} bath and $[Q,\infty]_{\text{II}} \cup [S,\infty]_{\text{II}}$ in CFT_2^{II} bath as depicted in the figure 10. Here the points P, Q have coordinates as $(u_0, v)_{\text{I,II}}$ in the cylinder coordinates and the points R, S are their corresponding TFD copies with coordinates $(u_0, -v + i\frac{\beta}{2})_{\text{I,II}}$. Note that in this case, the area term in the generalized entanglement entropy formula is vanishing as no island region is observed for this phase. The generalized entropy then involves only the effective term described by two two-point twist correlators and may be obtained to be

$$S_A = \frac{(c_{\text{I}} + c_{\text{II}})}{3}\log\left[\frac{\beta}{\pi\,\epsilon}\cosh\left(\frac{2\pi v}{\beta}\right)\right]. \tag{5.7}$$

JHEP11(2023)192

Doubly holographic description. The double holographic description for this phase corresponds to the RT surfaces being composed of two Hartman-Maldacena (HM) surfaces stretched between the endpoints of the semi-infinite intervals on the asymptotic boundaries as depicted in figure 10. The endpoints of the intervals are specified in the planer coordinates as $\tilde{x}_1(q_1^{\rm I})$ and $\tilde{x}_1(q_1^{\rm II})$ which may be obtained via the conformal maps eqs. (5.2) and (5.3). Consequently, in this phase the entanglement entropy corresponding to the HM surfaces may be obtained as

$$\begin{aligned} S_{\rm bulk} &= \frac{L_{\rm I}}{2G_N}\log\left[\frac{2\tilde{x}_1(q_1^{\rm I})}{\tilde{\epsilon}}\right] + \frac{L_{\rm II}}{2G_N}\log\left[\frac{2\tilde{x}_1(q_1^{\rm II})}{\tilde{\epsilon}}\right] \\ &= \frac{(L_{\rm I}+L_{\rm II})}{2G_N}\log\left[\frac{\beta}{\pi\epsilon}\cosh\left(\frac{2\pi v}{\beta}\right)\right]. \end{aligned} \tag{5.8}$$

Note that the UV cut-offs between the two coordinates are related by $\tilde{\epsilon}(u,v) = \epsilon\,\frac{2\pi\ell}{\beta}e^{\frac{2\pi u}{\beta}}$. The above expression matches identically with the result obtained in the effective $2d$ description.

5.2 Phase - II

Effective $2d$ description. Now we describe the second phase for the generalized entropy of semi-infinite subsystems $[P,\infty]_{\rm I}\cup[R,\infty]_{\rm I}$ in $\text{CFT}_2^{\rm I}$ bath and $[Q,\infty]_{\rm II}\cup[S,\infty]_{\rm II}$ in $\text{CFT}_2^{\rm II}$ bath. Note that, as earlier, the points P, Q are located at $(u_0,v)_{\rm I,II}$ in the cylinder coordinates and the points R, S are their corresponding TFD copies. This phase involves a conventional island region bounded by the QES $M\equiv(-a,v_a)_{\rm I,II}$ and $N\equiv(-a,-v_a+i\frac{\beta}{2})_{\rm I,II}$ on the JT brane leading to area terms in the generalized entanglement entropy. The effective terms in eq. (3.25) now involve four two-point twist correlators. The generalized entanglement entropy may then be obtained as

$$\begin{aligned} S_{\rm gen} =& \frac{4\pi\Phi_r}{\beta}\coth\left(\frac{2\pi a}{\beta}\right) + \frac{c_{\rm I}}{3}\log\left[\frac{1}{\cos\psi_{\rm I}}\right] + \frac{c_{\rm II}}{3}\log\left[\frac{1}{\cos\psi_{\rm II}}\right] \\ &+ \frac{(c_{\rm I}+c_{\rm II})}{3}\log\left[\frac{\left(e^{\frac{2\pi(-a-v_a)}{\beta}}-e^{\frac{2\pi(u_0-v)}{\beta}}\right)\left(e^{\frac{2\pi(-a+v_a)}{\beta}}-e^{\frac{2\pi(u_0+v)}{\beta}}\right)}{\frac{\pi\epsilon}{\beta}e^{\frac{2\pi u}{\beta}}\left(1-e^{\frac{-4\pi a}{\beta}}\right)}\right]. \end{aligned} \tag{5.9}$$

We first extremize the above over the time v_a of the QES to obtain the extremal value as

$$\partial_{v_a} S_{\rm gen} = 0 \quad\Rightarrow\quad v_a^* = v\,. \tag{5.10}$$

Subsequently, the extremization of the generalized entropy is performed over the location a of the QES to obtain the following equation

$$\partial_a S_{\rm gen} = 0 \quad\Rightarrow\quad \frac{\sinh\left(\frac{\pi(a-u)}{\beta}\right)}{\sinh\left(\frac{\pi(a+u)}{\beta}\right)} = \frac{12\pi\Phi_r}{\beta\,(c_{\rm I}+c_{\rm II})}\text{csch}\left(\frac{2\pi a}{\beta}\right). \tag{5.11}$$

where we have implemented $v_a^* = v$. The fine grained entanglement entropy for this configuration may be obtained by solving the above for the extremal value a^* and substituting it in eq. (5.9).

JHEP11(2023)192

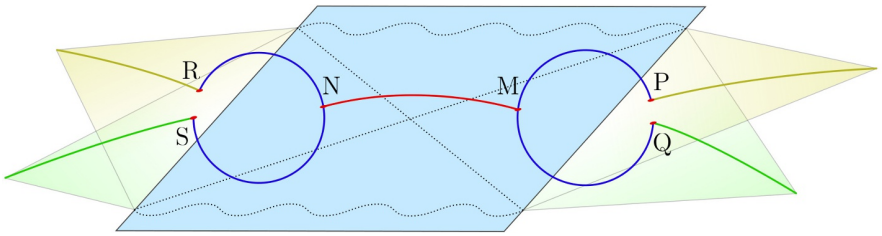

Figure 11. Schematics for the semi-infinite subsystem A in phase-II where we observe the island region NM on the JT brane in the effective $2d$ description.

Doubly holographic description. This subsection describes the doubly holographic computation of the entanglement entropy for the semi-infinite intervals in the dual $\text{CFT}_2^{\text{I,II}}$s at a finite temperature as depicted in figure 11. In particular, we compute the lengths of the RT surfaces homologous to the semi-infinite intervals. Similar to the previous case, we perform the computation in the planar coordinates[14] where the endpoints of the intervals are described by $(x_0, t_0)_{\text{I,II}}$ (and similarly for the TFD copies) in the dual $\text{CFT}_2^{\text{I,II}}$s, whereas the island point on the EOW brane is located at $(y,\, t_y)$. The length of the RT surface may now be obtained to be

$$\begin{aligned} d = 2L_{\text{I}} \log \left[\frac{(x_0 + y\sin\psi_{\text{I}})^2 + (t_0 - t_y)^2 + (y\cos\psi_{\text{I}})^2}{\epsilon\; y\cos\psi_{\text{I}}} \right] \\ + 2L_{\text{II}} \log \left[\frac{(x_0 + y\sin\psi_{\text{II}})^2 + (t_0 - t_y)^2 + (y\cos\psi_{\text{II}})^2}{\epsilon\; y\cos\psi_{\text{II}}} \right], \end{aligned} \tag{5.12}$$

where the factor 2 arises from the symmetry of the TFD state. After introducing transverse fluctuations on the EOW brane and identifying the dilaton, the entanglement entropy may be expressed as

$$\begin{aligned} S_{\text{bulk}} = \frac{2\Phi_r}{y} + \frac{L_{\text{I}}}{2G_N} \log \left(\frac{x_0^2 + 2x_0 y\sin\psi_{\text{I}} + y^2}{\epsilon\; y\;\cos\psi_{\text{I}}} \right) \\ + \frac{L_{\text{II}}}{2G_N} \log \left(\frac{x_0^2 + 2x_0 y\sin\psi_{\text{II}} + y^2}{\epsilon\; y\;\cos\psi_{\text{II}}} \right), \end{aligned} \tag{5.13}$$

where extremization over t_y has been performed to set $t_y = t_0$. The location of the island y may now be obtained by extremizing the above to obtain eq. (4.12) which may be transformed using the maps in eqs. (5.2) and (5.3) to obtain the corresponding extremization condition for the present scenario. Finally it may be observed that in the large tension limit the corresponding results match in the effective 2d theory.

5.3 Page curve

We now plot the Page curve for the entanglement entropy for the semi-infinite subsystem under consideration in the dual $\text{CFT}_2^{\text{I,II}}$s at a finite temperature in figure 12. We observe

[14] Note that it is convenient to work with the (x, t) coordinates in this case where we have a planar brane profile.

JHEP11(2023)192

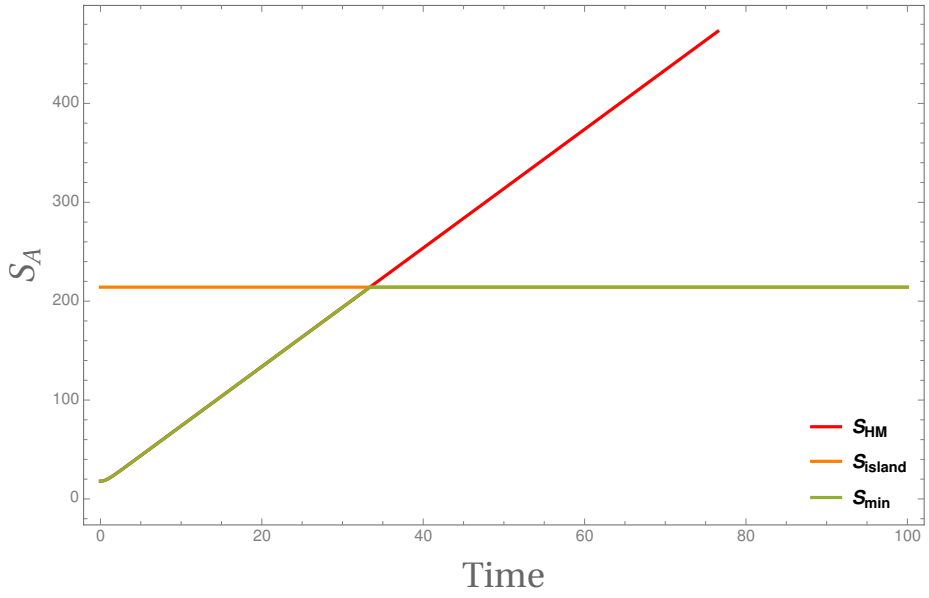

Figure 12. Page curve for semi-finite subsystem in the dual $\text{CFT}^{\text{I,II}}$. Here we have chosen $c_1 = 6, c_2 = 12, u_0 = 10, \beta = 2\pi, \epsilon = 0.1$.

that, similar to the conventional scenarios with a single CFT_2 bath, initially phase-I is dominant with a monotonically increasing entanglement entropy and finally the island saddle for phase-II takes over when the entropy gets saturated to a constant value. This is expected as the presence of the additional bath does not affect the radiation process of the JT black hole. It just provides an additional reservoir for the Hawking radiations to be collected.

6 Islands and replica wormholes: gravity coupled with two baths

In this section, we investigate the replica wormhole saddle for the gravitational path integral and reproduce the location of the conical singularity and the entanglement entropy. We first perform the analysis for the effective lower dimensional model obtained from the AdS/ICFT setup by integrating out the bulk degrees of freedom, namely the "brane+bath" picture with topological gravity on the AdS_2 brane. Later on, we will include JT gravity on the brane and obtain the location of the island and the corresponding fine-grained entropy.

The procedure for obtaining the replica wormhole solutions from the boundary curve in two-dimensional gravity coupled to flat bath requires solving the so called conformal welding problem [4, 42]. The schematics of the welding problem is sketched in figure 13. Essentially, the problem consists in finding a new Riemann surface out of two regions inside and outside of a disk which are described by different coordinate patches. Consider the regions parametrized by $|w| < 1$ and $|v| > 1$ which are glued together along their boundaries at $|v| = |w| = 1$, where the complex coordinates are described by

$$v = e^{y} = e^{\sigma + i\tau}, \quad w = e^{\gamma + i\theta}\,. \tag{6.1}$$

JHEP11(2023)192

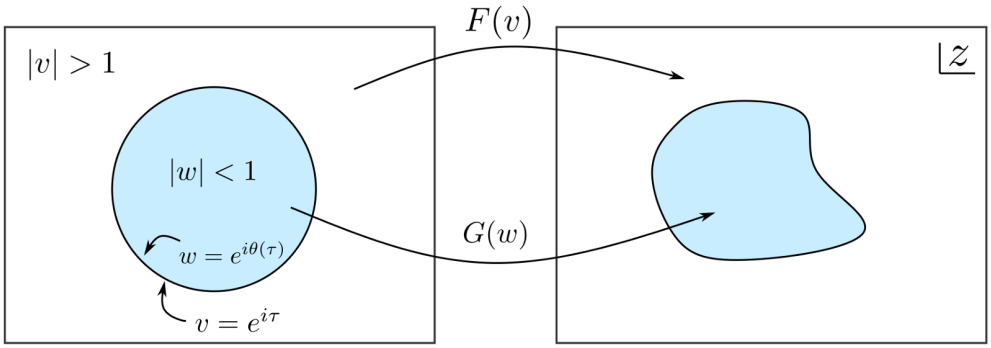

Figure 13. The conventional conformal welding problem [4]. The two disks $|v| > 1$ and $|w| < 1$ are glued in terms of the boundary mode $\theta(\tau)$, where $w = e^{i\theta(\tau)}$ and $v = e^{i\tau}$.

It is, in general, impossible to extend the coordinates w or v holomorphically beyond the respective boundary circles. However, by virtue of the Riemann mapping theorem, one can find two holomorphic functions F and G to establish another coordinate system z on a new Riemann surface such that the regions $|w| < 1$ and $|v| > 1$ are holomorphically mapped to the coordinate z. In other words, one requires

$$\begin{aligned} z &= G(w), && \text{for } |w| < 1 \\ z &= F(v), && \text{for } |v| > 1 \\ G\left(e^{i\theta(\tau)}\right) &= F\left(e^{i\tau}\right), && \text{for } |v| = |w| = 1\,. \end{aligned} \tag{6.2}$$

The problem of finding holomorphic $F(v)$ and $G(w)$ given the boundary mode $\theta(\tau)$ is termed the *conformal welding* problem. In the case of two dimensional gravity on a AdS_2 manifold coupled to a flat CFT_2 bath such a welding issue arises naturally [4, 42]. In the presence of dynamical gravity, the entanglement entropy for a subsystem is computed through the Lewkowycz-Maldacena procedure by considering an n-fold cover of the original manifold $\mathcal{M}$ [52]. For a replica symmetric saddle $\mathcal{M}_n$ to the gravitational path integral, it is convenient to quotient by the $\mathbb{Z}_n$ replica symmetry and consider a single manifold $\tilde{\mathcal{M}}_n = \mathcal{M}_n/\mathbb{Z}_n$. The orbifold $\tilde{\mathcal{M}}_n$ essentially describes a disk with conical singularities at which twist operators for the conformal matter theory are inserted. The metric on the interior manifold $\tilde{\mathcal{M}}_n$ may be described by a complex coordinate w as follows:

$$\mathrm{d}s^2 = e^{2\rho(w,\bar{w})}\mathrm{d}w\mathrm{d}\bar{w}, \quad \text{for} |w| < 1\,. \tag{6.3}$$

In a finite temperature configuration with $\tau \sim \tau + 2\pi$, in order to join the metric of the quotient manifold of the gravitating region to the flat space outside described by the exterior coordinates $v = e^y$, it is required to solve the conformal welding problem discussed above. In this case, the boundary mode $\theta(\tau)$ plays the role of the reparametrization mode in two-dimensional gravity [4].

6.1 Replica wormholes from AdS/ICFT

In this subsection, we focus on the replica wormhole solutions in the framework of AdS/ICFT discussed in [39] and briefly reviewed in section 2. In the effective lower dimensional sce-

JHEP11(2023)192

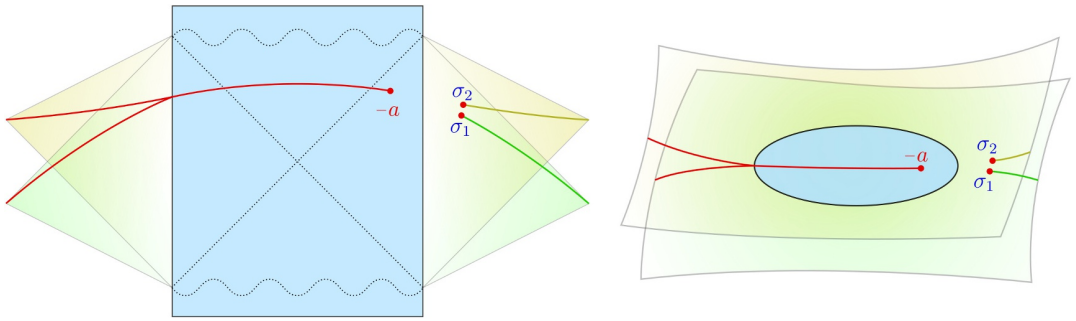

Figure 14. The single sided configuration in the Lorentzian signature (left) and in the Euclidean signature (right).

nario obtained from integrating out the bulk spacetimes on either side of the brane σ, we have two flat baths attached to the gravitational region on the EOW brane Σ which has a weakly gravitating metric in the large tension limit. There are two CFTs along the flat half lines which extends to the gravitating region where they interact via the weakly fluctuating metric. The schematics of the setup is sketched in figure 14.

As discussed earlier, for a quantum field theory coupled to dynamical gravity on a hybrid manifold, the replica trick to compute the entanglement entropy for a subsystem involves a replication of the original manifold in the replica index n. The normalized partition function $\mathbf{Z}_n$ on this replica manifold then computes the entanglement entropy as follows [4, 52]

$$S = -\partial_n \left(\frac{\log \mathbf{Z}_n}{n} \right) \Big|_{n=1} . \tag{6.4}$$

The partition function for the gravity region concerns a gravitational path integral which may be solved in the saddle-point approximation in the semi-classical regime by specifying appropriate boundary conditions. These saddles may be characterized by the nature of gluing of the individual replica copies. In particular, two specific choices will be of importance for our purposes, namely the Hawking saddle where the n-copies of the bath(s) are glued cyclically while gravity is filled in each copy individually, and the replica wormhole saddle in which along with the copies of the bath, gravitational regions are dynamically glued together. In these replica wormhole saddles, upon quotienting via the replica symmetry $\mathbb{Z}_n$, additional conical singularities dynamically appear at the fixed points of the replica symmetry in the orbifold theory.

The gravitational action on the orbifold $\tilde{\Sigma}_n$ obtained by quotienting the replicated EOW brane Σ_n is given by

$$\begin{aligned} -\frac{1}{n} I_{\text{grav}}[\tilde{\Sigma}_n] = & \sum_{k=\text{I,II}} \frac{L_k}{32\pi G_N} \int_\Sigma \mathrm{d}^2 y \sqrt{-\tilde{h}} \left[R^{(2)} - R^{(2)} \log \left(-\frac{L_k^2}{2} R^{(2)} \right) \right] \\ & - \left(1 - \frac{1}{n} \right) \sum_i S(w_i) \,, \end{aligned} \tag{6.5}$$

JHEP11(2023)192

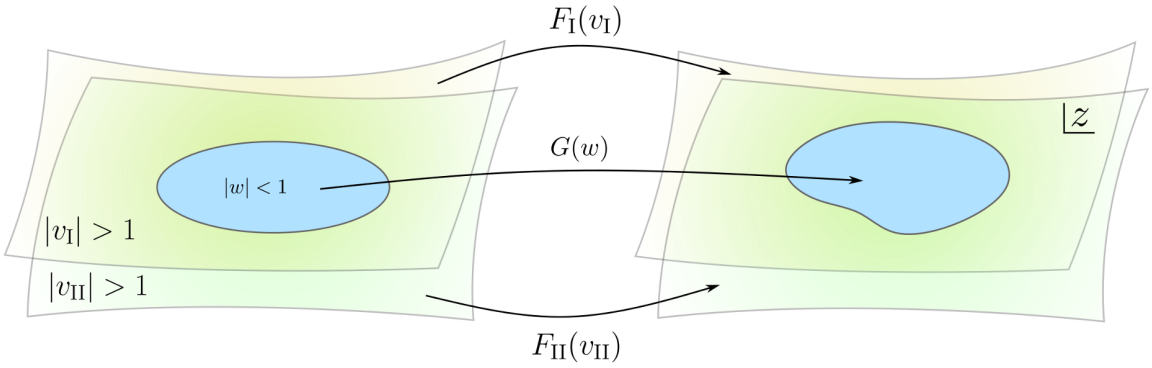

Figure 15. Conformal welding problem for our setup with two CFT_2 baths defined in the regions $|v_{\rm I}|>1$ and $|v_{\rm II}|>1$ which are coupled to gravity inside the circle $|w|<1$.

where $S(w_i)$ denotes the contributions from the dynamical conical singularities. In our case, this is just a constant given in eq. (3.16) with a vanishing dilaton term.

We choose the complex coordinate w to describe the gravity region inside the disk $|w|=1$. Furthermore, the baths outside the disk are described by the complex coordinates $v_k\,,(k=\text{I,II})$, in the spirit of eq. (6.1). Then the conformal welding problem sketched in figure 15 is reduced to the determination of the appropriate boundary mode $\theta(\tau)$. We consider two semi-infinite intervals in the bath $\text{CFT}_2^{\text{I,II}}$s as $[\sigma_1,\infty]_{\rm I}$ and $[\sigma_2,\infty]_{\rm II}$ and in the replica manifold twist operators are placed at the locations $v_{\rm I}=e^{\sigma_1}$ and $v_{\rm II}=e^{\sigma_2}$. Note that for the replica wormhole saddle, a dynamical conical singularity also appears at $w=e^{-a}$.

To proceed, we now require the energy flux equation at the interface of the gravitational region and the bath CFTs. The variation of the gravitational action with respect to the boundary mode is vanishing

$$-\frac{1}{n}\,\delta I_{\rm grav}=0\,. \tag{6.6}$$

On the other hand, the variation of the matter partition function $\mathbf{Z}_{\rm mat}$ with respect to the boundary mode leads to the following expression [4]

$$\delta\log\mathbf{Z}_{\rm mat}=i\int \mathrm{d}\tau\sum_{k=\text{I,II}}\left(T^{(k)}_{yy}-T^{(k)}_{\bar{y}\bar{y}}\right)\frac{\delta\theta(\tau)}{\theta'(\tau)} \tag{6.7}$$

Utilizing the above equations, the energy flux condition at the boundary may be expressed as follows

$$i\left[T^{(\text{I})}_{yy}(i\tau)-T^{(\text{I})}_{\bar{y}\bar{y}}(-i\tau)\right]+i\left[T^{(\text{II})}_{yy}(i\tau)-T^{(\text{II})}_{\bar{y}\bar{y}}(-i\tau)\right]=0\,. \tag{6.8}$$

Under the conformal map $y\to z=F_k(v_k)$, the energy momentum tensor transforms as

$$T^{(k)}_{yy}(i\tau)\to e^{2y}\left[\left(\frac{dF_k(e^y)}{dv_k}\right)^2T^{(k)}_{zz}-\frac{c_k}{24\pi}\left\{F_k(e^y),v_k\right\}\right],\quad k=\text{I,II} \tag{6.9}$$

JHEP11(2023)192

In the replicated geometry, the uniformization map for the conical singularities is given by $z \to \tilde{z} = z^{1/n}$ such that $T^{(k)}_{\tilde{z}\tilde{z}} = 0$ and the energy-momentum tensors for the two CFTs in the z-plane is given by

$$T^{(k)}_{zz} = -\frac{c_k}{24\pi}\left(1-\frac{1}{n^2}\right)\frac{1}{z^2}\,. \tag{6.10}$$

Therefore, the energy-flux condition in eq. (6.8) reduces to

$$0 = \sum_{k=\mathrm{I,II}} ie^{2i\tau}c_k\left[\frac{1}{2}\left(1-\frac{1}{n^2}\right)\left(\frac{F_k{}'(e^{i\tau})}{F_k(e^{i\tau})}\right)^2 + \left\{F_k(e^{i\tau}),e^{i\tau}\right\}\right] + \text{c.c.}\,. \tag{6.11}$$

Since the maps F_k depend on the gluing function $\theta(\tau)$, the above equation is in general hard to solve. However, one may solve it near $n = 1$ as described below.

For $n = 1$, the first term in the parenthesis of eq. (6.11) vanishes and the welding is trivial. Therefore, we may conclude that the maps F_k are well approximated near $n = 1$ by Möbius transformations of the form

$$z = F_k(v_k) = \frac{v_k - \mathcal{A}}{\mathcal{B}_k - v_k}, \quad \mathcal{A} = e^{-a}\ ,\ \mathcal{B}_{\mathrm{I}} = e^{\sigma_1}\ ,\ \mathcal{B}_{\mathrm{II}} = e^{\sigma_2} \tag{6.12}$$

It is straightforward to verify that these functions indeed map the branch points at $-a$ and $\sigma_{1,2}$ to $z = 0$ and $z = \infty$ respectively. Therefore, near $n \sim 1$, the energy flux condition becomes

$$c_{\mathrm{I}}\mathcal{F}_{\mathrm{I}} + c_{\mathrm{II}}\mathcal{F}_{\mathrm{II}} = 0\,, \tag{6.13}$$

where

$$\mathcal{F}_k = ie^{2i\tau}\left(\frac{F_k{}'\left(e^{i\tau}\right)}{F_k\left(e^{i\tau}\right)}\right)^2 + \text{c.c.} = ie^{2i\tau}\frac{(\mathcal{A}-\mathcal{B}_k)^2}{\left(e^{-i\tau}-\mathcal{A}\right)^2\left(e^{i\tau}-\mathcal{B}_k\right)^2} + \text{c.c.} \tag{6.14}$$

Now, performing a Fourier transformation in the above equation (restoring the temperature β), the expression for the $k = 1$ mode reads

$$\begin{aligned} 0 &= \int_0^\beta \mathrm{d}\tau\, e^{-\frac{2\pi i\tau}{\beta}}\left(c_{\mathrm{I}}\mathcal{F}_{\mathrm{I}} + c_{\mathrm{II}}\mathcal{F}_{\mathrm{II}}\right) \\ &= c_{\mathrm{I}}\left(\frac{\sinh\left[\frac{\pi(a-\sigma_1)}{\beta}\right]}{\sinh\left[\frac{\pi(a+\sigma_1)}{\beta}\right]}\right) + c_{\mathrm{II}}\left(\frac{\sinh\left[\frac{\pi(a-\sigma_2)}{\beta}\right]}{\sinh\left[\frac{\pi(a+\sigma_2)}{\beta}\right]}\right) \end{aligned} \tag{6.15}$$

In order to compare with the quantum extremal surface condition at zero temperature, we now take the $\beta \to \infty$ limit to obtain

$$0 = c_{\mathrm{I}}\left(\frac{a-\sigma_1}{a+\sigma_1}\right) + c_{\mathrm{II}}\left(\frac{a-\sigma_2}{a+\sigma_2}\right)\,, \tag{6.16}$$

which on solving for a gives

$$a^* = \frac{\left(c_{\mathrm{I}}-c_{\mathrm{II}}\right)\left(\sigma_1-\sigma_2\right) + \sqrt{4\left(c_{\mathrm{I}}+c_{\mathrm{II}}\right)^2\sigma_1\sigma_2 + \left(c_{\mathrm{I}}-c_{\mathrm{II}}\right)^2\left(\sigma_1-\sigma_2\right)^2}}{2\left(c_{\mathrm{I}}+c_{\mathrm{II}}\right)}\,. \tag{6.17}$$

The above expression is identical to the position of the quantum extremal surface obtained through extremizing the generalized entropy in [39].

JHEP11(2023)192

6.2 Replica wormholes with JT gravity coupled to two baths

With JT gravity on the EOW brane Σ, the energy flux condition at the boundary of the replicated geometry is modified and the conformal welding problem is a bit more involved. The variation of the gravitational action with respect to the boundary mode $\theta(\tau)$ no longer vanishes since in the case of JT gravity $\theta(\tau)$ serves as the "boundary graviton" [4]. The energy flux condition in the presence of JT gravity on the brane is then modified to [4, 10, 42]

$$\partial_\tau M = i\left[T^{(\mathrm{I})}_{yy}(i\tau) - T^{(\mathrm{I})}_{\bar{y}\bar{y}}(-i\tau)\right] + i\left[T^{(\mathrm{II})}_{yy}(i\tau) - T^{(\mathrm{II})}_{\bar{y}\bar{y}}(-i\tau)\right] \tag{6.18}$$

where M corresponds to the ADM mass of the gravitational theory which is related to the Schwarzian boundary action.

For the two single intervals $[\sigma_1,\infty]_{\mathrm{I}}$ and $[\sigma_2,\infty]_{\mathrm{II}}$ on $\mathrm{CFT}_2^{\mathrm{I,II}}$ baths, a conical singularity appears inside the gravity region on the orbifold theory $\Sigma_n/\mathbb{Z}_n$ at a point $-a$ and we need to consider the subsystems $[-\infty,-a]_{\mathrm{I}}\cup[\sigma_1,\infty]_{\mathrm{I}}$ and $[-\infty,-a]_{\mathrm{II}}\cup[\sigma_2,\infty]_{\mathrm{II}}$.[15] Once again, we will work with a finite temperature configuration with $\beta = 2\pi$. We may now uniformize the interior conical singularity at $w = \mathcal{A} = e^{-a}$ by utilizing the map

$$\tilde{w} = \left(\frac{w-\mathcal{A}}{1-\mathcal{A}\,w}\right)^{\frac{1}{n}}. \tag{6.19}$$

In the $\tilde{w}$ coordinates, the gravity region has the usual hyperbolic disk metric [4]

$$\mathrm{d}s^2_{\mathrm{in}} = \frac{4\mathrm{d}\tilde{w}\mathrm{d}\bar{\tilde{w}}}{\left(1-|\tilde{w}|^2\right)^2}. \tag{6.20}$$

In these coordinates we may set $\tilde{w} = e^{i\tilde{\theta}}$ at the boundary. Now using the Schwarzian composition rules, we may obtain the ADM mass of the spacetime to be [4]

$$\frac{\Phi_r}{4\pi}\left\{e^{i\tilde{\theta}},\tau\right\} = \frac{\Phi_r}{4\pi}\left[\left\{e^{i\theta},\tau\right\} + \frac{1}{2}\left(1-\frac{1}{n^2}\right)R(\theta)\right], \tag{6.21}$$

where the function $R(\theta)$ contains the information about the branch point $-a$ as follows

$$R(\theta) = -\frac{(1-\mathcal{A}^2)^2(\partial_\tau\theta)^2}{|1-\mathcal{A}\,e^{i\theta}|^4}. \tag{6.22}$$

Now, utilizing eqs. (6.11), (6.18) and (6.21), the energy flux condition at the boundary becomes

$$\begin{aligned} &-12\Phi_r\,\partial_\tau\left[\left\{e^{i\theta},\tau\right\} + \frac{1}{2}\left(1-\frac{1}{n^2}\right)R(\theta)\right] \\ &\qquad = \sum_{k=\mathrm{I,II}} i\,e^{2i\tau}c_k\left[\frac{1}{2}\left(1-\frac{1}{n^2}\right)\left(\frac{F_k{}'(e^{i\tau})}{F_k(e^{i\tau})}\right)^2 + \left\{F_k(e^{i\tau}),e^{i\tau}\right\}\right] + \text{c.c.} \end{aligned} \tag{6.23}$$

[15] Note that the local geometry at the point $-a$ on the replica manifold Σ_n is completely smooth.

JHEP11(2023)192

The above relation is quite complicated as the map F depends implicitly on the gluing function $\theta(\tau)$. Nevertheless, as earlier, we may solve it near $n \sim 1$ as follows. Near $n \sim 1$, we may expand the boundary mode $\theta(\tau)$ as follows [4]

$$e^{i\theta(\tau)} = e^{i\tau}\left[1 + i\delta\theta(\tau)\right], \tag{6.24}$$

where $\delta\theta(\tau)$ is of order $(n-1)$. Next we use the following relation [4]

$$e^{2i\tau}\left\{F_k, e^{i\tau}\right\} = -\frac{1}{2}(1+H)(\delta\theta''' + \delta\theta'), \tag{6.25}$$

where H is the Hilbert transform[16] which projects out the negative frequency modes of $\delta\theta$. Note that, except for in the Schwarzian term $\{F_k, e^{i\tau}\}$, the functions F_k appear with a factor of $(n-1)$ in eq. (6.23) and we may keep only up to the zeroth order solutions given in eq. (6.12). Restoring the temperature dependence utilizing the scaling $\Phi_r \to \frac{2\pi\Phi_r}{\beta}$ and Fourier transforming to the k basis, the $k=1$ mode requires

$$\int_0^\beta \mathrm{d}\tau\, e^{-\frac{2\pi i\tau}{\beta}}\left[c_{\mathrm{I}}\mathcal{F}_{\mathrm{I}} + c_{\mathrm{II}}\mathcal{F}_{\mathrm{II}} - \frac{24\pi\Phi_r}{\beta}\partial_\tau R(\tau)\right] = 0 \tag{6.27}$$

which leads to the condition

$$c_{\mathrm{I}}\left(\frac{\sinh\left[\frac{\pi(a-\sigma_1)}{\beta}\right]}{\sinh\left[\frac{\pi(a+\sigma_1)}{\beta}\right]}\right) + c_{\mathrm{II}}\left(\frac{\sinh\left[\frac{\pi(a-\sigma_2)}{\beta}\right]}{\sinh\left[\frac{\pi(a+\sigma_2)}{\beta}\right]}\right) = \frac{12\pi\Phi_r}{\beta}\mathrm{csch}\left(\frac{2\pi a}{\beta}\right) \tag{6.28}$$

In the $\beta \to \infty$ limit, this reduces to a cubic equation in a as follows

$$c_{\mathrm{I}}\left(\frac{a-\sigma_1}{a+\sigma_1}\right) + c_{\mathrm{II}}\left(\frac{a-\sigma_2}{a+\sigma_2}\right) = \frac{6\Phi_r}{a} \tag{6.29}$$

The above equation is easily solved for a but the solutions are not quite illuminating. Instead, we take the simplifying limit $\sigma_1 = \sigma_2 = \sigma$ to get the quadratic equation

$$a(a-\sigma) - \frac{6\Phi_r}{(c_{\mathrm{I}}+c_{\mathrm{II}})}(a+\sigma) = 0\,. \tag{6.30}$$

Solving for the position of the conical singularity a, we obtain

$$a^* = \frac{(c_{\mathrm{I}}+c_{\mathrm{II}})\,\sigma + 6\Phi_r + \sqrt{((c_{\mathrm{I}}+c_{\mathrm{II}})\,\sigma + 6\Phi_r)^2 + 24\,(c_{\mathrm{I}}+c_{\mathrm{II}})\,\sigma\Phi_r}}{2\,(c_{\mathrm{I}}+c_{\mathrm{II}})} \tag{6.31}$$

which is identical to the position of the QES obtained in section 4.1.

[16] The Hilbert transform is defined through the action

$$H\cdot e^{im\tau} = -\mathrm{sgn}(m)e^{im\tau}, \quad H\cdot 1 = 0\,. \tag{6.26}$$

JHEP11(2023)192

7 Summary and discussion

In this article, we have investigated the entanglement structure of various bipartite states in a hybrid manifold where a JT gravity is coupled to two non-gravitating CFT_2 baths. To this end, we first construct this hybrid theory through a dimensional reduction of a $3d$ geometry. The $3d$ geometry is comprised of a fluctuating EOW brane acting as an interface between two distinct AdS_3 geometries. Performing a partial Randall-Sundrum reduction in the neighbourhood of the fluctuating brane results in JT gravity on the EOW brane. Furthermore, utilizing the usual AdS/CFT correspondence on the remaining wedges of the two AdS_3 geometries leads to two non-gravitating CFT baths on two half lines. In the limit of large brane tension, we obtain the $2d$ effective theory of JT gravity coupled to conformal matter on the hybrid "brane+baths" manifolds.

Furthermore, we have provided a prescription for computing the generalized Rényi entropy for a subsystem in this hybrid manifold. In particular, for this scenario where the JT gravity is coupled to two CFT_2 baths, the dominant replica wormhole saddle is modified to provide two independent mechanisms to obtain an island region. Other than the conventional origin of the island region where the degrees of freedom for the CFT in the gravitational region is shared by bath CFTs, we also observe cases where island region is captured for CFT^{I} even though no bath degrees of freedom is considered. We have called such regions as the induced islands, as the subsystem purely in CFT^{II} induces an island region even for CFT^{I}. In the doubly holographic perspective this phenomena corresponds to the double-crossing geodesic where the RT surface crosses from AdS^{II} to AdS^{I} and returns to AdS^{II}.

Subsequently, we obtain the entanglement entropy for subsystems comprised of semi-infinite and finite intervals in $\text{CFT}_2^{\text{I,II}}$ coupled to extremal as well as eternal JT black holes. We perform computations from the effective $2d$ perspective using the generalized entanglement entropy formula and find agreement with the doubly holographic computation in the large tension limit of the EOW brane for all the cases. We also plot Page curves for the different configurations of the subsystems and observe transitions between different phases of the entanglement entropy.

We have also performed the so called conformal welding problem for the replica wormhole saddle in the effective "brane+bath" scenario and obtained the location of the island for semi-infinite subsystems in the baths. To this end, we begin with the lower dimensional effective picture obtained from the AdS/ICFT setup discussed in [39] and reproduce the QES result. Subsequently, this is extended to the case with JT gravity on the EOW brane which substantiate the island computations for the corresponding configuration.

There are several future directions to explore. For finite intervals in the baths coupled to JT gravity, the location of the islands may be obtained through the conformal welding problem with the replica wormhole by extending of the analysis in [42]. It will be interesting to explore the nature of mixed state entanglement in Hawking radiation from the JT black hole via different entanglement and correlation measures such as the reflected entropy [53], the entanglement negativity [54], the entanglement of purification [55] and the balanced partial entanglement [56]. Furthermore, our setup can be extended to include

JHEP11(2023)192

holographic models of interface CFTs which involve two interface branes separating three bulk regions [57]. A partial dimensional reduction on different bulk wedges would result in two fluctuating JT branes with black holes which interact through the CFT_2 baths on a hybrid seagull-like geometry. This provides yet another exotic model of Hawking radiation which may lead to new insights for the information loss problem.

Acknowledgments

The work of GS is partially supported by the Dr Jagmohan Garg Chair Professor position at the Indian Institute of Technology, Kanpur.

A Second order fluctuations

In this appendix, we investigate the second order terms in the brane fluctuations $\tilde{\rho}_k(t,y)$ and obtain corrections to the on-shell action eq. (3.9) describing the effective intermediate perspective along the lines of [34–36]. We assume that the brane fluctuations $\tilde{\rho}_k$ depend on both the coordinates (t,y). The normal vectors to eq. (3.1) are given by

$$n_\mu^{(\text{I})} = \mathcal{N}_\text{I}\left(1, \frac{\partial\tilde{\rho}_\text{I}}{\partial t}, \frac{\partial\tilde{\rho}_\text{I}}{\partial y}\right), \quad n_\mu^{(\text{II})} = \mathcal{N}_\text{II}\left(1, -\frac{\partial\tilde{\rho}_\text{II}}{\partial t}, -\frac{\partial\tilde{\rho}_\text{II}}{\partial y}\right), \tag{A.1}$$

where the normalizations $\mathcal{N}_k$ contributes only in higher order terms.

The trace of the extrinsic curvatures of the EOW brane embedded in each AdS_3 geometry may now be computed as

$$\begin{aligned} K_k = \nabla_\mu n^{\mu\,(k)} &= \frac{1}{\sqrt{-g}}\partial_\mu\left(\sqrt{-g}\, g^{\mu\nu} n_\nu^{(k)}\right) \\ &= \frac{2}{L_k}\tanh\left(\frac{\rho_k^0 + (-1)^k\tilde{\rho}_k}{L_k}\right) + \frac{(-1)^k y^2}{L_k^2\cosh^2\left(\frac{\rho_k^0+(-1)^k\tilde{\rho}_k}{L_k}\right)}\left[\frac{\partial^2\tilde{\rho}_k}{\partial t^2} - \frac{\partial^2\tilde{\rho}_k}{\partial y^2}\right], \end{aligned} \tag{A.2}$$

which at the leading order, matches with the trace of the extrinsic curvature in eq. (3.5). For the hypersurface parametrized by $(\rho_0 \mp \tilde{\rho}_{\text{I,II}}, t, y)$, we may construct the tangent vectors $e_a^{\mu\,(\text{I})} = \frac{\partial x_\text{I}^\mu}{\partial y^a}$ and $e_a^{\mu\,(\text{II})} = \frac{\partial x_\text{II}^\mu}{\partial y^a}$ to obtain the induced metric on the brane (cf. eq. (3.6))

$$h_{ab} = g^\text{I}_{\mu\nu}\frac{\partial x_\text{I}^\mu}{\partial y^a}\frac{\partial x_\text{I}^\mu}{\partial y^b} = g^\text{II}_{\mu\nu}\frac{\partial x_\text{II}^\mu}{\partial y^a}\frac{\partial x_\text{II}^\mu}{\partial y^b}. \tag{A.3}$$

The determinant of the induced metric expanded upto second order in $\tilde{\rho}_k$ reads

$$\sqrt{-h} = \frac{L_k^2}{y^2}\cosh^2\left(\frac{\rho_k^0 + (-1)^k\tilde{\rho}_k}{L_k}\right) - \frac{1}{2}\left[\left(\frac{\partial\tilde{\rho}_k}{\partial t}\right)^2 - \left(\frac{\partial\tilde{\rho}_k}{\partial y}\right)^2\right] \tag{A.4}$$

Now, integrating the Einstein-Hilbert action upto second order in $\tilde{\rho}_k$ and adding the contributions from the Gibbons-Hawking boundary terms and the tension term, we obtain the

JHEP11(2023)192

following correction to the effective action for the lower dimensional theory,

$$\begin{aligned} I_{\text{dilaton}} = &-\frac{1}{8\pi G_N}\int \mathrm{d}^2y\sqrt{-g^{(2)}}\frac{\tanh\left(\frac{\rho_{\rm I}^0}{L_{\rm I}}\right)}{2L_{\rm I}^3\cosh^2\left(\frac{\rho_{\rm I}^0}{L_{\rm I}}\right)}\left(2\tilde{\rho}_{\rm I}^2+y^2\left[-\left(\frac{\partial\tilde{\rho}_{\rm I}}{\partial t}\right)^2+\left(\frac{\partial\tilde{\rho}_{\rm I}}{\partial y}\right)^2\right]\right)\\ &+\frac{1}{8\pi G_N}\int \mathrm{d}^2y\sqrt{-g^{(2)}}\frac{\tanh\left(\frac{\rho_{\rm II}^0}{L_{\rm II}}\right)}{2L_{\rm II}^3\cosh^2\left(\frac{\rho_{\rm II}^0}{L_{\rm II}}\right)}\left(2\tilde{\rho}_{\rm II}^2+y^2\left[-\left(\frac{\partial\tilde{\rho}_{\rm II}}{\partial t}\right)^2+\left(\frac{\partial\tilde{\rho}_{\rm II}}{\partial y}\right)^2\right]\right)\\ = &-\frac{1}{8\pi G_N}\int \mathrm{d}^2y\sqrt{-g^{(2)}}\left[\frac{T_{\rm I}}{2}\nabla_\mu\tilde{\rho}_{\rm I}\,\nabla^\mu\tilde{\rho}_{\rm I}+\frac{T_{\rm I}}{\ell_{\text{eff}}^2}\tilde{\rho}_{\rm I}^2-\frac{T_{\rm II}}{2}\nabla_\mu\tilde{\rho}_{\rm II}\,\nabla^\mu\tilde{\rho}_{\rm II}-\frac{T_{\rm II}}{\ell_{\text{eff}}^2}\tilde{\rho}_{\rm II}^2\right], \end{aligned} \tag{A.5}$$

where ℓ_{eff} is given in eq. (3.10), the metric $g^{(2)}_{ab}$ is related to h_{ab} through eqs. (3.3) and (3.6), and we have defined

$$T_k \equiv \frac{1}{L_k}\tanh\left(\frac{\rho_k^0}{L_k}\right). \tag{A.6}$$

In the following, we will set $\ell_{\text{eff}}=1$ for brevity. Introducing,

$$\psi(y) = \frac{T_{\rm I}}{\sqrt{T_{\rm I}+T_{\rm II}}}\tilde{\rho}_{\rm I}+\frac{T_{\rm II}}{\sqrt{T_{\rm I}+T_{\rm II}}}\tilde{\rho}_{\rm II}\,, \tag{A.7}$$

and subsequently performing a Weyl transformation of the $2d$ metric

$$g^{(2)}_{ab}\to e^{\frac{T_{\rm I}T_{\rm II}}{T_{\rm I}+T_{\rm II}}(\tilde{\rho}_{\rm II}-\tilde{\rho}_{\rm I})}g^{(2)}_{ab}\,, \tag{A.8}$$

the complete induced action may be simplified to obtain the JT gravity coupled to a massive scalar field as follows

$$\begin{aligned} I_{\text{total}} = I_{\text{topological}} &+\frac{1}{16\pi G_N^{(2)}}\int_\Sigma \mathrm{d}^2y\sqrt{-g^{(2)}}\,\Phi(y)\left(R^{(2)}+2\right)\\ &+\frac{1}{8\pi G_N}\int_\Sigma \mathrm{d}^2y\sqrt{-g^{(2)}}\left[\frac{1}{2}\nabla_\mu\psi\nabla^\mu\psi+\psi^2\right]. \end{aligned} \tag{A.9}$$

Interestingly, we may gauge out the scalar field entirely by performing yet another Weyl transformation,

$$g^{(2)}_{ab}\to e^{-\psi}g^{(2)}_{ab}\,, \tag{A.10}$$

thereby reproducing the JT gravity action as in eq. (3.9).

JHEP11(2023)192

References

[1] G. Penington, *Entanglement Wedge Reconstruction and the Information Paradox*, *JHEP* **09** (2020) 002 [arXiv:1905.08255] [INSPIRE].

[2] G. Penington, S.H. Shenker, D. Stanford and Z. Yang, *Replica wormholes and the black hole interior*, *JHEP* **03** (2022) 205 [arXiv:1911.11977] [INSPIRE].

[3] A. Almheiri, R. Mahajan, J. Maldacena and Y. Zhao, *The page curve of Hawking radiation from semiclassical geometry*, *JHEP* **03** (2020) 149 [arXiv:1908.10996] [INSPIRE].

[4] A. Almheiri et al., *Replica Wormholes and the Entropy of Hawking Radiation*, *JHEP* **05** (2020) 013 [arXiv:1911.12333] [INSPIRE].

[5] A. Almheiri, R. Mahajan and J. Maldacena, *Islands outside the horizon*, arXiv:1910.11077 [INSPIRE].

[6] A. Almheiri, R. Mahajan and J.E. Santos, *Entanglement islands in higher dimensions*, *SciPost Phys.* **9** (2020) 001 [arXiv:1911.09666] [INSPIRE].

[7] D.N. Page, *Information in black hole radiation*, *Phys. Rev. Lett.* **71** (1993) 3743 [hep-th/9306083] [INSPIRE].

[8] D.N. Page, *Average entropy of a subsystem*, *Phys. Rev. Lett.* **71** (1993) 1291 [gr-qc/9305007] [INSPIRE].

[9] D.N. Page, *Time Dependence of Hawking Radiation Entropy*, *JCAP* **09** (2013) 028 [arXiv:1301.4995] [INSPIRE].

[10] K. Suzuki and T. Takayanagi, *BCFT and Islands in two dimensions*, *JHEP* **06** (2022) 095 [arXiv:2202.08462] [INSPIRE].

[11] J. Sully, M. Van Raamsdonk and D. Wakeham, *BCFT entanglement entropy at large central charge and the black hole interior*, *JHEP* **03** (2021) 167 [arXiv:2004.13088] [INSPIRE].

[12] M. Rozali et al., *Information radiation in BCFT models of black holes*, *JHEP* **05** (2020) 004 [arXiv:1910.12836] [INSPIRE].

[13] H.Z. Chen et al., *Quantum Extremal Islands Made Easy, Part I: Entanglement on the Brane*, *JHEP* **10** (2020) 166 [arXiv:2006.04851] [INSPIRE].

[14] H.Z. Chen et al., *Quantum Extremal Islands Made Easy, Part II: Black Holes on the Brane*, *JHEP* **12** (2020) 025 [arXiv:2010.00018] [INSPIRE].

[15] G. Grimaldi, J. Hernandez and R.C. Myers, *Quantum extremal islands made easy. Part IV. Massive black holes on the brane*, *JHEP* **03** (2022) 136 [arXiv:2202.00679] [INSPIRE].

[16] H. Geng and A. Karch, *Massive islands*, *JHEP* **09** (2020) 121 [arXiv:2006.02438] [INSPIRE].

[17] H. Geng et al., *Information Transfer with a Gravitating Bath*, *SciPost Phys.* **10** (2021) 103 [arXiv:2012.04671] [INSPIRE].

[18] H. Geng, S. Lüst, R.K. Mishra and D. Wakeham, *Holographic BCFTs and Communicating Black Holes*, *JHEP* **08** (2021) 003 [arXiv:2104.07039] [INSPIRE].

[19] H. Geng et al., *Entanglement phase structure of a holographic BCFT in a black hole background*, *JHEP* **05** (2022) 153 [arXiv:2112.09132] [INSPIRE].

[20] H. Geng et al., *Inconsistency of islands in theories with long-range gravity*, *JHEP* **01** (2022) 182 [arXiv:2107.03390] [INSPIRE].

JHEP11(2023)192

[21] F. Deng, J. Chu and Y. Zhou, *Defect extremal surface as the holographic counterpart of Island formula*, *JHEP* **03** (2021) 008 [arXiv:2012.07612] [INSPIRE].

[22] J. Chu, F. Deng and Y. Zhou, *Page curve from defect extremal surface and island in higher dimensions*, *JHEP* **10** (2021) 149 [arXiv:2105.09106] [INSPIRE].

[23] T. Takayanagi, *Holographic Dual of BCFT*, *Phys. Rev. Lett.* **107** (2011) 101602 [arXiv:1105.5165] [INSPIRE].

[24] M. Fujita, T. Takayanagi and E. Tonni, *Aspects of AdS/BCFT*, *JHEP* **11** (2011) 043 [arXiv:1108.5152] [INSPIRE].

[25] J. Kastikainen and S. Shashi, *Structure of holographic BCFT correlators from geodesics*, *Phys. Rev. D* **105** (2022) 046007 [arXiv:2109.00079] [INSPIRE].

[26] T. Li, M.-K. Yuan and Y. Zhou, *Defect extremal surface for reflected entropy*, *JHEP* **01** (2022) 018 [arXiv:2108.08544] [INSPIRE].

[27] D. Basu, H. Parihar, V. Raj and G. Sengupta, *Defect extremal surfaces for entanglement negativity*, *Phys. Rev. D* **108** (2023) 106005 [arXiv:2205.07905] [INSPIRE].

[28] Y. Shao, M.-K. Yuan and Y. Zhou, *Entanglement Negativity and Defect Extremal Surface*, arXiv:2206.05951 [INSPIRE].

[29] Y. Lu and J. Lin, *The Markov gap in the presence of islands*, *JHEP* **03** (2023) 043 [arXiv:2211.06886] [INSPIRE].

[30] D. Basu, J. Lin, Y. Lu and Q. Wen, *Ownerless island and partial entanglement entropy in island phases*, arXiv:2305.04259 [INSPIRE].

[31] R. Jackiw, *Lower Dimensional Gravity*, *Nucl. Phys. B* **252** (1985) 343 [INSPIRE].

[32] C. Teitelboim, *Gravitation and Hamiltonian Structure in Two Space-Time Dimensions*, *Phys. Lett. B* **126** (1983) 41 [INSPIRE].

[33] T.J. Hollowood and S.P. Kumar, *Islands and Page Curves for Evaporating Black Holes in JT Gravity*, *JHEP* **08** (2020) 094 [arXiv:2004.14944] [INSPIRE].

[34] F. Deng, Y.-S. An and Y. Zhou, *JT gravity from partial reduction and defect extremal surface*, *JHEP* **02** (2023) 219 [arXiv:2206.09609] [INSPIRE].

[35] H. Geng et al., *Jackiw-Teitelboim Gravity from the Karch-Randall Braneworld*, *Phys. Rev. Lett.* **129** (2022) 231601 [arXiv:2206.04695] [INSPIRE].

[36] H. Geng, *Aspects of AdS_2 quantum gravity and the Karch-Randall braneworld*, *JHEP* **09** (2022) 024 [arXiv:2206.11277] [INSPIRE].

[37] E. Verheijden and E. Verlinde, *From the BTZ black hole to JT gravity: geometrizing the island*, *JHEP* **11** (2021) 092 [arXiv:2102.00922] [INSPIRE].

[38] J. Kumar Basak et al., *Page curve for entanglement negativity through geometric evaporation*, *SciPost Phys.* **12** (2022) 004 [arXiv:2106.12593] [INSPIRE].

[39] T. Anous, M. Meineri, P. Pelliconi and J. Sonner, *Sailing past the End of the World and discovering the Island*, *SciPost Phys.* **13** (2022) 075 [arXiv:2202.11718] [INSPIRE].

[40] C. Bachas, J. de Boer, R. Dijkgraaf and H. Ooguri, *Permeable conformal walls and holography*, *JHEP* **06** (2002) 027 [hep-th/0111210] [INSPIRE].

[41] E. Sharon and D. Mumford, *2D-Shape Analysis Using Conformal Mapping*, *Int. J. Comput. Vision* **70** (2006) 55.

JHEP11(2023)192

[42] K. Goto, T. Hartman and A. Tajdini, *Replica wormholes for an evaporating 2D black hole*, *JHEP* **04** (2021) 289 [arXiv:2011.09043] [INSPIRE].

[43] J. Maldacena, D. Stanford and Z. Yang, *Conformal symmetry and its breaking in two dimensional Nearly Anti-de-Sitter space*, *PTEP* **2016** (2016) 12C104 [arXiv:1606.01857] [INSPIRE].

[44] S. Fallows and S.F. Ross, *Islands and mixed states in closed universes*, *JHEP* **07** (2021) 022 [arXiv:2103.14364] [INSPIRE].

[45] K. Skenderis and S.N. Solodukhin, *Quantum effective action from the AdS / CFT correspondence*, *Phys. Lett. B* **472** (2000) 316 [hep-th/9910023] [INSPIRE].

[46] X. Dong, X.-L. Qi, Z. Shangnan and Z. Yang, *Effective entropy of quantum fields coupled with gravity*, *JHEP* **10** (2020) 052 [arXiv:2007.02987] [INSPIRE].

[47] S. Ryu and T. Takayanagi, *Holographic derivation of entanglement entropy from AdS/CFT*, *Phys. Rev. Lett.* **96** (2006) 181602 [hep-th/0603001] [INSPIRE].

[48] J.D. Brown and M. Henneaux, *Central Charges in the Canonical Realization of Asymptotic Symmetries: An Example from Three-Dimensional Gravity*, *Commun. Math. Phys.* **104** (1986) 207 [INSPIRE].

[49] M. Banados, *Three-dimensional quantum geometry and black holes*, *AIP Conf. Proc.* **484** (1999) 147 [hep-th/9901148] [INSPIRE].

[50] M.M. Roberts, *Time evolution of entanglement entropy from a pulse*, *JHEP* **12** (2012) 027 [arXiv:1204.1982] [INSPIRE].

[51] T. Shimaji, T. Takayanagi and Z. Wei, *Holographic Quantum Circuits from Splitting/Joining Local Quenches*, *JHEP* **03** (2019) 165 [arXiv:1812.01176] [INSPIRE].

[52] A. Lewkowycz and J. Maldacena, *Generalized gravitational entropy*, *JHEP* **08** (2013) 090 [arXiv:1304.4926] [INSPIRE].

[53] S. Dutta and T. Faulkner, *A canonical purification for the entanglement wedge cross-section*, *JHEP* **03** (2021) 178 [arXiv:1905.00577] [INSPIRE].

[54] P. Calabrese, J. Cardy and E. Tonni, *Entanglement negativity in extended systems: A field theoretical approach*, *J. Stat. Mech.* **1302** (2013) P02008 [arXiv:1210.5359] [INSPIRE].

[55] T. Takayanagi and K. Umemoto, *Entanglement of purification through holographic duality*, *Nature Phys.* **14** (2018) 573 [arXiv:1708.09393] [INSPIRE].

[56] Q. Wen, *Balanced Partial Entanglement and the Entanglement Wedge Cross Section*, *JHEP* **04** (2021) 301 [arXiv:2103.00415] [INSPIRE].

[57] S.A. Baig and A. Karch, *Double brane holographic model dual to 2d ICFTs*, *JHEP* **10** (2022) 022 [arXiv:2206.01752] [INSPIRE].

JHEP11(2023)192